UNIVERSITY OF CALIFORNIA SAN DIEGO

Elucidating Novel Factors in the Plant Guard Cell CO_2 Signaling Pathway:

A Complementary Forward Genetic Screen in *Arabidopsis thaliana*

A Thesis submitted in partial satisfaction of the requirements for the degree Master of Science

in

Biology

by

Kelsey Jankay Swink

Committee in charge:

Professor Julian Schroeder, Chair
Professor Yunde Zhao, Co-Chair
Professor Martin Yanofsky

2021

The thesis of Kelsey Jankay Swink is approved, and it is acceptable in quality and form for publication on microfilm and electronically.

University of California San Diego

2021

DEDICATION

I dedicate this Thesis to my amazing family: Katy, Dad, Victoria, and Casper Swink.

To Mom: Thank you for being my motivation to do great things, teaching me how to be a strong, intelligent woman, and always making sure I know that I can achieve anything I put my mind to.

To Dad: Thank you for always supporting me in anything I want to pursue, being someone I can confide in when I feel like the world is too scary, and teaching me about life.

To Toria: Thank you to my best friend in the entire world for being my closest ally, my biggest supporter, and favorite human being.

To Casper: Woof woof!

Your endless love, support, and inspiration has propelled me through my academic career, uplifting me during tough times and celebrating with me after. There are no other people I would rather have at my side. I love you all so much and I'm so excited to share this moment with you.

EPIGRAPH

Nothing in life is to be feared,
it is only to be understood.
Now is the time to understand more,
so that we may fear less.

Marie Curie

TABLE OF CONTENTS

LIST OF FIGURES

LIST OF TABLES

ACKNOWLEDGEMENTS

I would like to thank Dr. Julian Schroeder for giving me the opportunity to be a part of his laboratory for 3 years. Thank you for being such a great PI, encouraging me to do my best, and providing such an incredible lab environment to learn and grow as a scientist!

My thanks also extend to my committee members, Drs. Yunde Zhao and Martin Yanofsky for their time and support serving on my committee.

Thank you to my mentor, Dr. Guillaume Dubeaux, for his guidance, support, and encouragement throughout my time in the lab. Thank you for training me, showing me interesting experiments, teaching me how to design a project, giving me the confidence to be independent, being there for me when I had questions, and, most of all, shaping me into the scientist I am today. I will miss working with you, but know I made a lifelong friend.

I would also like to thank all the Schroeder Lab members who were there for me when I asked questions, my peers who struggled with me, and all the friends I made along the way.

Thank you to Dr. Andrew Cooper, for being my first friend in lab, helping to make my years as a Grad Student so memorable, and being there with me through the biggest achievements of my academic career! Your help and support have been invaluable.

I would like to acknowledge and thank my incredible team, Dr. Guillaume Dubeaux, Sabrina Lin, Logan Chinn, Katie Lu, Elizabeth Bottenberg, and Angela Liu for working with me and for their contributions to my project. Specifically thank you to Guillaume, Sabrina, and Logan for helping me with my blinded stomatal index/density assays and their continuation of my project. Thank you to Elizabeth Bottenberg for her help with the high-throughput forward genetic screen. Thank you to Angela Liu and Sabrina Lin for their help with the re-screen. I would like to acknowledge Dr. Guillaume Dubeaux for allowing the presentation of the data used in **Figure 5**.

I would like to give huge thank you to everyone who helped me with proofreading: Julian Schroeder, Guillaume Dubeaux, Andrew Cooper, Victoria Swink, Andrej Pervan, Milena Pervan, Titus Hartmann, and David Swink.

I would most like to thank my friends, family, and my partner for their constant encouragement, emotional support, and cheering me on. My most sincere gratitude goes to my family: Katy, David, Victoria, and Casper Swink. Thank you for your never-ending support, love, encouragement, and being my #1 fans. I would never have made it this far without you. I love you all so much.

ABSTRACT OF THE THESIS

Elucidating Novel Factors in the Plant CO_2 Signaling Pathway: A Complementary Forward Genetic Screen in *Arabidopsis thaliana*

by

Kelsey Jankay Swink

Master of Science in Biology

University of California San Diego, 2021

Professor Julian Schroeder, Chair
Professor Yunde Zhao, Co-Chair

Climate change mitigation is at the forefront of global discussion, thus the study of plant responses to atmospheric CO_2 is of great ecophysiological importance. Stomata, the pores of the plant, open and close in response to varying atmospheric CO_2 levels. Therefore, it is important to investigate transduction pathways that mediate stomatal responses to CO_2 variation. Since elevated CO_2 reduces stomatal apertures, this response is of particular interest considering the rapidly rising atmospheric CO_2 levels. While plants are considered to be a promising organism for atmospheric CO_2 mitigation, still some components of the CO_2 response pathway are not well understood,

specifically the CO_2 sensor in guard cells for both stomatal movements and stomatal development. This study aims to elucidate novel factors in the plant guard cell CO_2 signaling pathway. This project consists of a complementary forward genetic screen and preliminary characterization of a robust candidate identified from the screen. The complementary forward genetic screen, performed in *Arabidopsis thaliana,* was conducted using two tools: the gain-of-function FOX-hunting plant line approach and a homologous gene silencing artificial-microRNA (amiRNA) plant line approach. Both FOX-hunting and amiRNA lines were screened in conditions that specifically favored the identification of mutants involved in stomatal movement or stomatal development response to CO_2. A total of 43 amiRNA and 19 FOX-line candidate plants were identified and sequenced. One candidate repeatedly identified in the screen was an amiRNA line targeting two leucine-rich repeat (LRR) family genes in the *A. thaliana* genome: AT3G43740 and AT5G21090. This LRR candidate showed a partially impaired gas exchange response and a lower stomatal count compared to the wild-type, indicating the observed phenotype is a product of a stomatal development mutation. The remaining candidate plants identified from the screen will be characterized in the future, using this preliminary characterization as precedent, with aim to further the understanding of the guard cell CO_2 signal transduction pathway in plants.

1. INTRODUCTION:

Climate change caused by manmade greenhouse gas emissions is one of the most pressing issues of the century (Mora et al., 2018). The main greenhouse gas that contributes to the global warming effect is carbon dioxide (CO_2) (Mora et al., 2018). Among the first to record the steady rising CO_2 levels and correlate this increase to global warming was Charles David Keeling (Marx et al., 2017). Much of his work contributed to the ongoing data record of atmospheric CO_2 concentration over time, dubbed the Keeling Curve; the data has been compiled and recorded daily by the Scripps Institute of Oceanography at the University of California San Diego since 1958 (Keeling et al., 1976; SIO, 2020). The atmospheric CO_2 concentration has been rising at an alarming rate since the industrial revolution and is currently at its highest level in human history, at over 410 ppm (SIO, 2020).

Atmospheric CO_2 concentration is predicted to double during this century (Leakey et al., 2009). Plants have the ability to sequester CO_2 from the atmosphere, which makes them a promising candidate for mitigating the problem of global warming (Nowak et al., 2002). Therefore, it is important to understand the implications that rising CO_2 will have on plant development and physiology (Woodward, 1987; Bailey-Serres et al., 2019). Plants are eukaryotic organisms that perform photosynthesis, the process of using sunlight to convert water and CO_2 into glucose, releasing O_2 as a byproduct (Engineer et al., 2016). They also undergo transpiration, during which water is released into the atmosphere, cooling the plant (Engineer et al., 2016). Plants are sessile organisms, which means they have distinct mechanisms to deal with constantly changing environmental cues, such as drought, heat, or CO_2 levels (Engineer et al., 2016). In plants, the leaf epidermis contains stomata, pores through which gas exchange occurs (Schulze et al., 1973;

Willmer & Fricker, 1996; Ceciliato et al., 2019). Plants can allow CO_2 into the leaf intracellular space and use it for photosynthesis, as well as release water and O_2 (Santelia et al., 2016). In dicots, a singular stomate is made up of two guard cells (Hetherington & Woodward, 2003; Hashimoto et al., 2006). These guard cells have vacuoles, which are filled with water, and the water content in these vacuoles creates turgor pressure (Kim et al., 2010; Azoulay-Shemer et al., 2015). Water follows the concentration gradient into and out of the guard cells. The movement of potassium (K+), anions (Cl-, malate), and organic solutes (sucrose) across the guard cell membrane is responsible for mediating turgor pressure, the change in water content inside the cells (Willmer & Fricker, 1996; Negi et al., 2008; Dong et al., 2018). The degree of vacuole swelling causes guard cell stiffening or relaxation; more water in the vacuoles stiffens the cell walls of the guard cells, opening up the stomate and vice versa (Azoulay-Shemer et al., 2015; Engineer et al., 2016). Therefore, the aperture of the stomatal pore is dependent on the turgor pressure in the guard cells (Kim et al., 2010; Azoulay-Shemer et al., 2015). Stomatal movements occur in response to many different factors (Weyers et al., 1983). While stomata can open and close in response to environmental stimuli, such as abscisic acid and blue light, CO_2 can also regulate stomatal movements (Hauser et al., 2017; Hiyama et al., 2017). Intracellular signaling pathways sense CO_2 changes and respond by regulating stomatal movements to optimize CO_2 influx, water loss, and plant growth under various conditions (Hu et al., 2010). More specifically, increased [CO_2] triggers stomatal closure, while reduced [CO_2] results in stomatal opening (Lawson et al., 2014).

Plant photosynthesis and transpiration produce sizable daily gaseous fluctuations within the plant (Lawson et al., 2014). However, if the CO_2 concentration in the atmosphere is high, the concentration gradient between the leaf intracellular space and the atmosphere drives CO_2 to enter the leaves (Kim et al., 2010). Thus, the rising atmospheric CO_2 leads to an increase in leaf

intracellular CO_2 concentration, which triggers stomatal closure (Zheng et al., 2019). This stomatal closure results in a decreased transpiration rate and thus reduced water-flux out of the leaves, creating warmer conditions within the plant, and ultimately, causing stress on the organism (Schulze et al., 1973; Kim et al., 2010). If persistent, the reduced transpiration rate may have a substantial adverse effect on plant growth, water-use efficiency, heat stress response, and gas exchange (Kim et al., 2010).

In plant genetic studies, a flowering plant *Arabidopsis thaliana* is often used as a model organism because of its smaller genome relative to other plants, making it more advantageous in molecular genetics (Koornneef et al., 2010; Woodward & Bartel, 2018). This model organism is also favored due to its short generation time, small size, self-pollinating abilities, and abundant seed production (Koornneef et al., 2010; Woodward & Bartel, 2018).

However, even though *Arabidopsis thaliana* has a smaller, fully sequenced genome, its genome, like all plants, contains many large gene families and subfamilies (Arabidopsis Genome Initiative, 2000). These families have many genes with partial or fully functional overlap, meaning there can be multiple genes responsible for the same function (Hauser et al., 2013; Hauser et al., 2019; Cutler and McCourt, 2005). This genetic redundancy is considered to be the primary obstacle in detecting robust phenotypes in single-gene knockout mutants; knocking out or deleting one gene may not result in an observable phenotype because another gene could compensate for this loss (Ma et al., 2009; Park et al., 2009).

Many genes have been identified and characterized to play a role in the CO_2 signaling pathway that encode factors such as the protein kinases MPK4, MPK12, HT1, OST1, CBC1, CBC2, and the pseudo-kinase GHR1 (Hõrak & Woodward, 2003; Hashimoto et al., 2006; Jakobson et al., 2016; Tõldsepp et al., 2018; Zhang et al., 2018). Ion channels, for example,

AtSLAC1, AtALMT12/QUAC1, SLAH3, and RHC1 play a role as well (Negi et al., 2008; Demir et al., 2013; Wang et al., 2015; Zhang et al., 2018). To be sensed and used by plants, CO_2 is converted to bicarbonate (HCO3-) by carbonic anhydrases like βCA1 and βCA4, which then binds to the SLAC1 anion channel (Negi et al., 2008; Hu et al., 2010; Engineer et al., 2014; Wang et al., 2015; Zhang et al., 2018). Upstream of SLAC1, OST1 has been implicated in the CO_2 signaling pathway as well, responding to high CO_2 exposure (Xue et al., 2011; Hsu et al., 2018). HCO3- activates OST1 and induces stomatal closure (Xue et al., 2011; Hsu et al., 2018). Multiple CO_2 signal transduction factor mutants have been found to be impaired in stomatal movements, resulting in canopy leaf temperature differences compared to wild-type (WT) controls in various CO_2 conditions (Matrosova et al., 2015).

However, there are still missing pieces from this CO_2 sensing and perception transduction pathway; specifically, the factors that interact to mediate CO_2 sensing for stomatal movements and development are still unknown (Schroeder et al., 2001; Bergmann et al., 2004; Kollist et al., 2014; Engineer et al., 2014; Zhang et al., 2018). An obstacle with elucidating novel factors in *A. thaliana* is that there are many genes that could have functional overlap or genetic redundancy, essentially masking the phenotype in screens using single-knockout mutants that do not account for homologous genes compensating for the knockout of the single gene (Ma et al., 2009; Park et al., 2009).

Therefore, a tool was developed by the Schroeder Lab to allow for genetic screening of these putative, functionally redundant genes by utilizing artificial-microRNA (amiRNA) technology (Hauser et al., 2013). This tool aims to utilize RNA-based gene silencing that has been observed in organisms in nature (Carbonell et al., 2014). The canonical silencing RNA motif is where a small RNA sequence (either an siRNA or miRNA) selectively degrades the

complementary mRNA strands, decreasing expression of the corresponding gene (Ossowski et al., 2008). SiRNAs are perfectly complementary to the target strand, as opposed to miRNAs, which can have multiple mRNA targets due to their different degrees of complementation to the genomic DNA (Carbonell et al., 2014). Alternatively, amiRNAs are custom RNA-silencing technology utilizing artificially engineered miRNA constructs that can be designed to target the mRNAs from more than one gene of choice (Schwab et al., 2006; Ossowski et al., 2008). The tool designed in the Schroeder lab uses an amiRNA computational design approach to create a genome-wide, family-specific database of amiRNAs (Hauser et al., 2013). This homologous gene silencing amiRNA technology allows for the generation of knockdown lines expressing amiRNAs that selectively target putative functionally redundant genes (Hauser et al., 2013). Using this amiRNA database, the authors generated a seed resource library of over 14,000 amiRNA expressing lines for screening homologous genes with putative functional redundancy (Hauser et al., 2019). In amiRNAs, the miRNA motif allows these amiRNAs to target multiple gene mRNAs because miRNAs have less specificity than siRNAs, which overcomes this tight specificity constriction (Carbonell et al., 2014).

Conversely, another tool called the FOX-hunting system (**F**ull-length cDNA **O**ver-e**X**pressing gene hunting system) was developed by the Matsui lab as a gain-of-function approach to overcome off-target expression often seen with the use of transcriptional enhancers (Ichikawa et al., 2006). Transcriptional enhancers are not necessarily specific to one gene and can sometimes drive the expression of genes that were not intended to be expressed, resulting in off-target expression that can lead to a complex phenotype (Ichikawa et al., 2006). Instead, this tool was designed to allow for overexpression of a gene of interest, while minimizing off-target gene expression by replacing transcriptional promoters with an exogenous promoter, as well as

expressing cDNA lines ectopically by artificially inducing abnormal gene expression in a different tissue, cell type, or developmental stage. (Ichikawa et al., 2006). This type of expression can allow a gene that is not typically expressed in a tissue to be phenotypically distinct from wild-type and more easily identifiable in a screen (Ichikawa et al., 2006). The authors used the exogenous 35S promoter isolated from the cauliflower mosaic virus (CAV) (Ichikawa et al., 2006; Amack & Antunes, 2020). Since CAV-35S is an exogenous promoter, it can drive the overexpression of a gene of interest without the off-target effects seen with endogenous promoters, overcoming the limitations of transcriptional enhancers (Ichikawa et al., 2006; Amack & Antunes, 2020). Their team generated over 10,000 independent full-length cDNAs of randomly selected *A. thaliana* genes, which were introduced to an expression vector with a 35S promoter and transformed into wild-type *A. thaliana* (Ichikawa et al., 2006). These FOX-hunting lines produce overexpression of genes that can be used to screen for a phenotype of interest in *A. thaliana* from a gain-of-function approach (Ichikawa et al., 2006).

Tools like these can be used to screen plants to identify novel genes and contribute to the current literature in plant physiology. The current literature suggests that there exists a mechanism for CO_2 response in guard cells that correspond to the stomatal opening and closure mechanistic response (Schroeder et al., 2001). Additionally, CO_2 has been known to affect stomatal development by decreasing stomatal density in response to prolonged elevated CO_2 (Xu et al., 2016). However, some of the gene elements of the molecular and cellular signaling mechanisms that mediate CO_2 control of stomatal function, specifically the factors involved with CO_2 sensing in both stomatal movements and stomatal development, remain unknown (Zhang et al., 2018). Therefore, these tools allow us to elucidate genes using a novel approach that can overcome the obstacle of functional genetic redundancy as well as provide a complementary gain-of-function

method to screen for candidates that otherwise could not be identified with typical loss-of-function screens.

This thesis aims to identify novel candidates that could be implicated in the CO_2 signaling pathway by performing a high-throughput complementary genetic screen in *A. thaliana* designed using these two tools: a homologous gene silencing artificial miRNA (amiRNA) plant line approach using the Phantom Database library and a gain-of-function approach using the Full-length cDNA Over-eXpressing (FOX-hunting) system. This complementary genetic screen was designed to detect genes that may have been challenging to identify previously due to functional genetic redundancy masking the phenotype. This thesis presents the candidates identified from this screen, as well as preliminary characterization data of one candidate. Future studies will aim to characterize all candidates and their role in the plant CO_2 signaling pathway.

2. RESULTS:

2.1 Identification of candidate lines with altered canopy leaf temperatures compared to wild-type: Primary high-throughput forward genetic screen of 14,000 amiRNA lines and 20,496 FOX lines conducted in low CO_2 conditions

A high-throughput complementary genetic screen was conducted in *Arabidopsis thaliana* with two approaches: homologous gene silencing using artificial microRNAs (amiRNAs) and the gain-of-function FOX-hunting system (**F**ull-length cDNA **O**ver-e**X**pressing gene hunting system). The Phantom Database (PhantomDB) contains 2,002,149 amiRNAs (phantomdb.ucsd.edu). Using PhantomDB, a library of 22,000 amiRNAs with 18,117 targets and 10 sub-libraries (130 pools) was created and yielded 14,000 individual T2 amiRNA lines (Hauser & Ceciliato et al., 2019). These 14,000 individual T2 amiRNA lines were screened. 124 amiRNA pools were screened with approximately 90 lines per pool, with each line represented by approximately 20 seeds. The

FOX-hunting system is a library of 10,000 independent *Arabidopsis* full-length cDNAs, 21 sub-libraries and 410 pools, giving us 20,496 individual FOX lines (Ichikawa et al., 2006). These 20,496 FOX-hunting lines were screened. In total, 410 FOX-hunting pools were screened with approximately 50 lines per pool, with each line represented by approximately 8 seeds.

For both the gain-of-function and homologous gene silencing artificial miRNA (amiRNA) approaches, T2 generation plants were grown at ambient CO_2, 400 parts per million (ppm), for 3-4 weeks prior to being screened after transfer to a low ambient CO_2 condition, of 150 ppm for 2 hours and then visualized via infrared (IR) imaging. Representative IR images are shown for candidate LC2 (Figure 1).

The screen was optimized to use low CO_2 conditions to look for a warm canopy leaf temperature phenotype. We would expect WT-like plants to exhibit stomatal opening when exposed to low CO_2, to allow for more gas exchange when less CO_2 is available. This stomatal opening cools the leaves, therefore an impaired stomatal opening mechanism or decreased stomatal density number would result in a warmer leaf temperature. Controls used with candidate lines were *ht1-2*, a high leaf temperature amiRNA mutant, and HsMYO, our amiRNA WT control. *Ht1-2* (HIGH LEAF TEMPERATURE 1-2) is the warm canopy leaf temperature control used in this screen because it is a known mutant that has impaired stomatal movements in response to different CO_2 concentrations (Hashimoto et al., 2006). HsMYO is the WT control used in our screen because it contains an amiRNA that targets the human myosin 2 gene, which means there is no target to knock down in our model, *Arabidopsis* (Hauser et al., 2013).

For amiRNA lines, canopy leaf temperatures warmer than the control plant WT (amiRNA-HsMYO) were isolated and grown to the next generation (T3). For FOX lines, canopy leaf

temperatures warmer than the control plant WT (COL-0) were isolated and grown to the next generation (T3). *Ht1-2* was used as a warm canopy leaf control.

Thermal Imaging with a FLIR Infrared (IR) camera was used to identify warm candidate plants from the 34,496 total lines. This thermography visualization, directly following 2hr low CO_2 treatment (150 ppm), allows us to have an early idea of plant lines that could be implicated in an impaired stomatal movement or a stomatal development phenotype in response to CO_2 changes. High-throughput screening was achieved by sowing 20 seedlings per pot with control plants in the middle.

A representative IR image of the amiRNA high-throughput screen shows that a putative candidate from pool 4 was qualitatively selected due to a distinctly warm canopy leaf temperature closely resembling the warm control (*ht1-2*) (Figure 1A). Figure 1B shows that the juvenile plants have their first true leaves, are healthy, and are homogeneously sown around the perimeter of the pot. The warm putative candidate (Figure 1A) was isolated and propagated to the next generation. Quantitative investigation comparing the plant canopy leaf temperatures revealed that the putative amiRNA candidate had a canopy leaf temperature exceeding 20°C and was warmer than both controls (Figure 1C). Canopy leaf temperature was determined using ImageJ software by taking a temperature measurement from each leaf of the plant and averaging all four leaves to give a "whole plant temperature" (Figure 1C).

Several candidates were isolated from this primary screen: 75 amiRNA candidates and 99 FOX candidates. The putative candidate screening rate was 0.05% which indicates that the screen was very selective. The high selectivity means that validated candidates will be the most robust of the screened population.

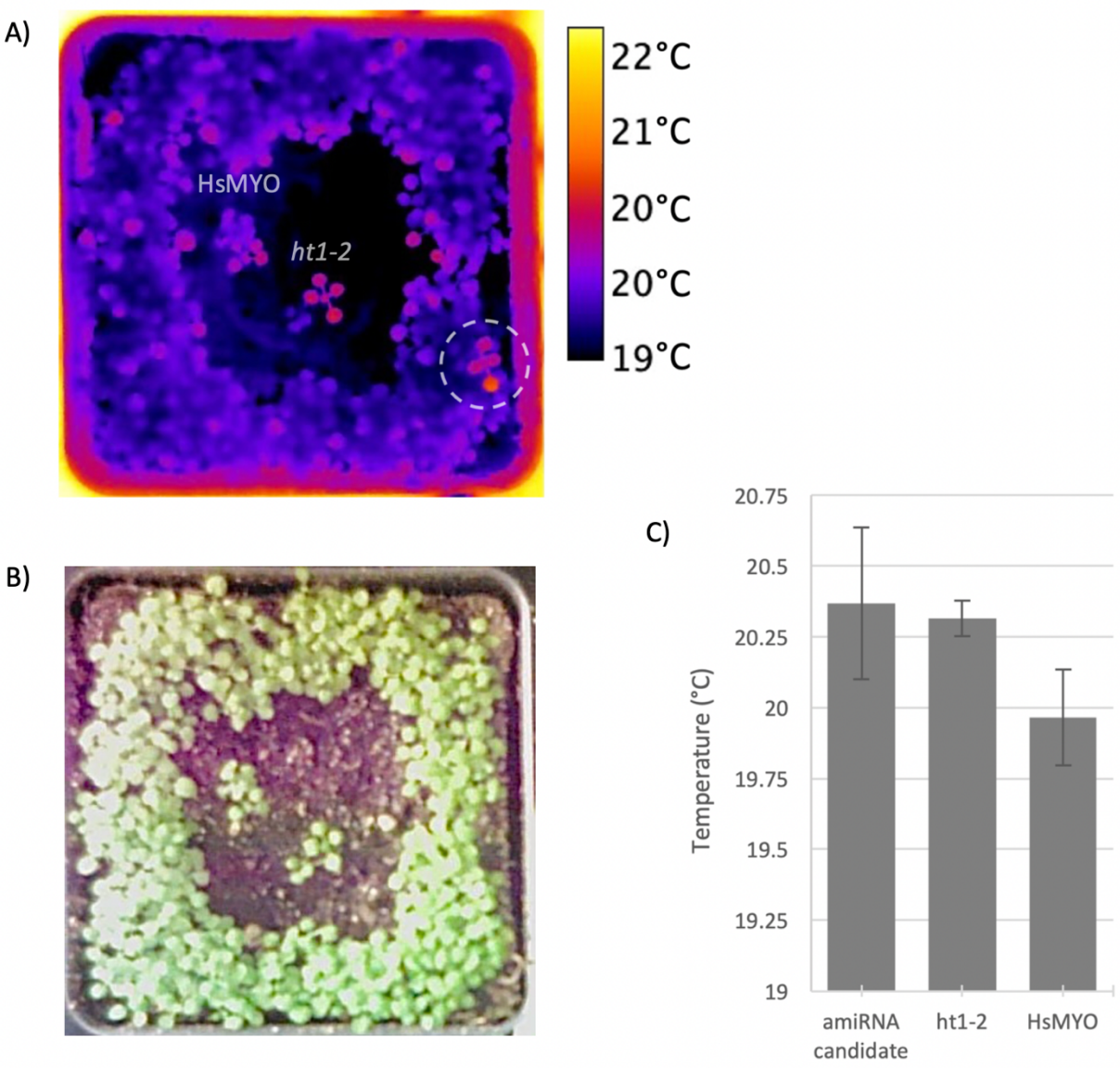

Figure 1: Representative IR image of amiRNA high-throughput screen.

Candidate pool 4 was grown around the perimeter of the pot. Controls, HsMYO and *ht1-2,* were grown in the center. A) T2 generation high-throughput IR pictures were captured immediately following low CO_2 incubation for 2 hours. B) Brightfield image extracted from the IR camera shows healthy T2 *Arabidopsis* plants. C) The whole plant canopy leaf temperature was generated by averaging all four leaf temperatures. Difference in canopy leaf temperature for amiRNA candidate vs. controls shown in a bar graph. The putative amiRNA candidate had a canopy leaf temperature exceeding 20°C and was warmer than both controls. Error bars represent the standard deviation.

2.2 Validation of candidate phenotypes in T3 generation: Secondary re-screen in low CO_2 at next generation confirmed 43 amiRNA and 19 FOX candidates

A secondary re-screen was conducted with the isolated 75 amiRNA candidates and 99 FOX candidates at the next generation (T3). Immediately prior to IR imaging, plants were incubated in low CO_2 (150 ppm) for 2 hours. A representative IR image of the candidate LC2 plants, alongside controls HsMYO and *ht1-2* (hot leaf mutant), show that the candidates were as warm as *ht1-2* (Figure 2A). Figure 2B shows that the plants were healthy, suggesting that the observed warm phenotype was only a result of the low CO_2 incubation. Quantitative investigation comparing the plant canopy leaf temperatures revealed that both LC2 plants had a canopy leaf temperature exceeding 21°C and were warmer than HsMYO (Figure 2C). Canopy leaf temperature was determined using ImageJ software by taking a temperature measurement from each leaf of the plant and averaging all individual leaf temperatures together to represent a "whole plant temperature" (Figure 2C).

This re-screen used only two candidate plants per pot and one of each of the aforementioned control plants, for a total of four plants per pot. This resulted in a clear picture of the warm canopy leaf temperature phenotype. Robust candidates were confirmed at this stage, taking into consideration the silencing effect at subsequent generations (T3). This secondary re-screen in low CO_2 at the T3 generation validated 43 amiRNA and 19 FOX candidates for potential CO_2-insensitive phenotypes.

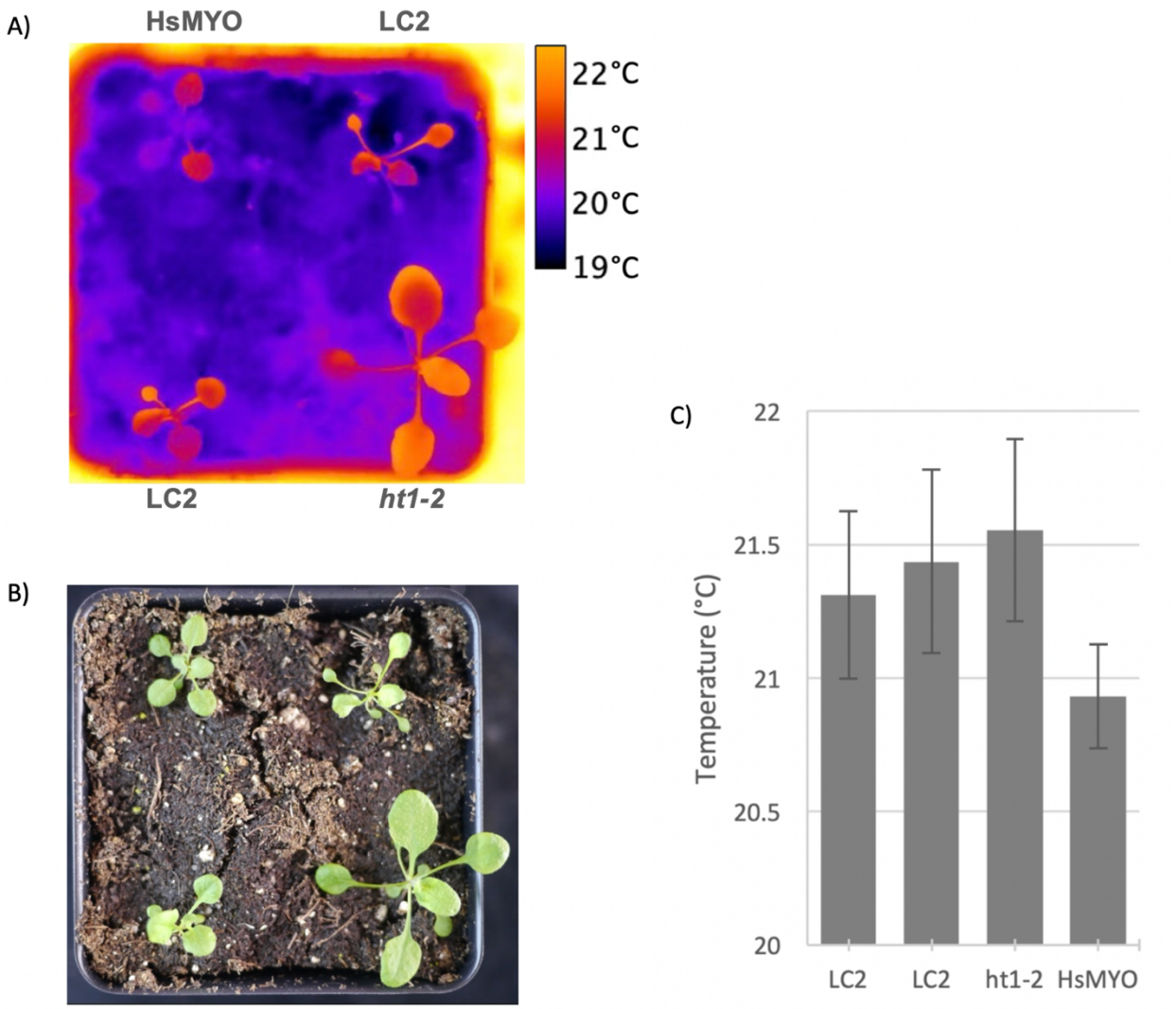

Figure 2: Re-screen IR analysis shows differences in canopy leaf temperature between candidates and controls.

Five-week-old *Arabidopsis* plants were grown and imaged. Candidate LC2 is pictured on the top right and bottom left of the pot; controls are pictured on the top left (amiRNA-HsMYO) and bottom right (*ht1-2*) of the pot. A) T3 generation validation IR picture captured immediately following low CO_2 exposure for 2 hours. B) Brightfield image of the same candidate pot shows the plant phenotypes without IR. C) The whole plant canopy leaf temperature was generated by averaging all four leaf temperatures. Difference in canopy leaf temperature shown in the bar graph. The LC2 candidates have canopy leaf temperatures exceeding 21°C and closely resemble the warm control, *ht1-2*, both via qualitative eye observation and via quantitative ImageJ temperature analysis. Error bars represent the standard deviation.

2.3 Identification of candidate genes

Genomic DNA (gDNA) was extracted from all 43 amiRNA candidates, the amiRNA insert was amplified, and the amplicon was sent for sequencing. All sequences identified can be found in Table 1. The primers designed for amplification can be found in Table 2. Then, all amiRNA sequences were run through WMD3 to identify the loci targeted by the amiRNA insert. All target loci are listed in Table 1. Primers were designed for GateWay Cloning and re-transformation (Table 2).

Preliminary characterization was pursued for the candidates that were the most robust, validated at the T3 generation, and sequenced. Therefore, T2 generation plants for candidates LC17, LC24, LC27, LC28, LC35, LC42, LC43 and control amiRNA-HsMYO (WT) were grown and imaged at 4-weeks-old (Figure 3). Five plants per genotype were grown and one representative image for each genotype is shown. The rosettes pictured in Figure 3 show the variation between WT amiRNA-HsMYO and the various amiRNA candidate plants. Interestingly, LC27 displays a wide rosette variation within its genotype at the T3 generation (Figure 4). LC27.1 is closest in phenotype to WT HsMYO, although it appears to have more waxy coating than HsMYO. LC27.2 and LC 27.4 both display narrow curled leaves and a dramatic rosette spiral compared to WT HsMYO. LC 27.3 also closely resembles WT HsMYO but is dwarfed in size. LC27.5 resembles WT HsMYO in both color and size but has more leaf curl compared to WT.

Retransformation in Colombia-0 (COL0) is ongoing for these candidates in order to obtain T1 generation seeds of our amiRNA candidates. The transformations produce a different insertion event while still maintaining the same amiRNA sequence, which can be used to confirm that the observed candidate phenotype is indeed a result of the amiRNA targeted knockdown rather than the insertion event itself. T-DNA insertion lines were also ordered and received. These lines have

a T-DNA inserted into the same loci targeted by the amiRNA, with aim to render gene silencing independent of amiRNA and determine whether the phenotype persists with this alternative gene disruption.

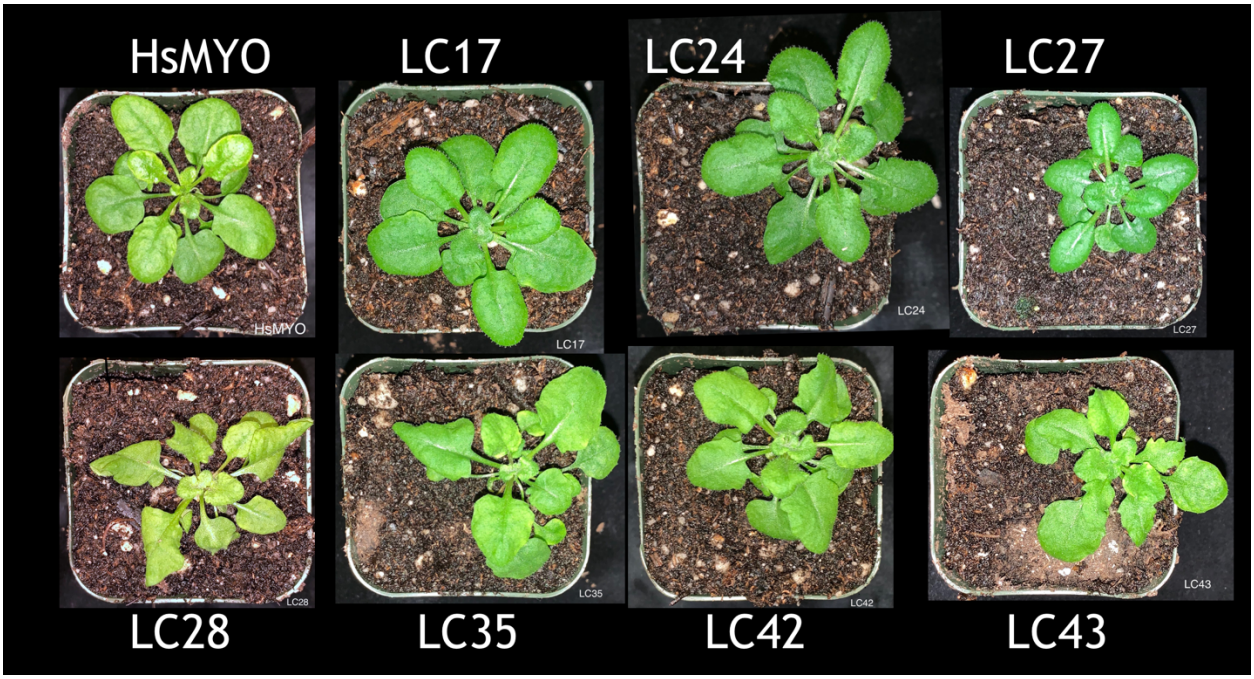

Figure 3: Images taken of the control (HsMYO) and candidates LC17, LC24, LC 27, LC 28, LC35, LC42, and LC43 show the rosette phenotype of the amiRNA candidate plants.

Five plants for each candidate (T3) were grown and imaged at 5-weeks-old (only one representative image for each genotype group shown).

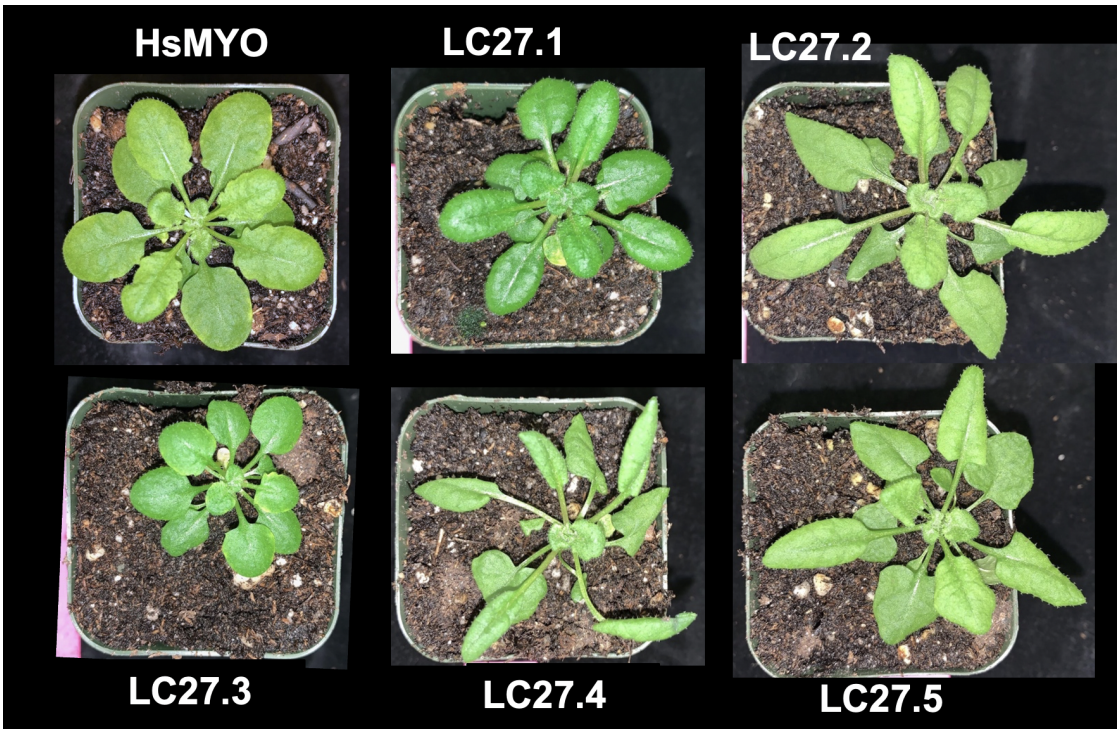

Figure 4: Images taken of the control HsMYO and amiRNA candidate plant LC27 show the rosette phenotype of the plants.

Candidate LC27 exhibits variation in rosette phenotype compared to HsMYO. Five plants for each candidate (T3) were grown and imaged at 5-weeks-old (only one representative image for HsMYO is shown; all images for candidate LC27 are shown).

Table 1: Table of all amiRNA candidates identified through a high-throughput loss of function genetic screen in low CO_2 conditions. Leftmost column matches with PhantomDB (phantomdb.ucsd.edu). Sequencing data, library, and loci shown in latter columns.

Pool	Code	Basta resistance	Round 2 screening (T3 gen)	PCR band (1119F/1129R)	Sequencing results (1123F)	amiRNA	Library	Locus silenced	Col0 re-transformation
PKR	LC1	yes	Robust	yes	yes	TTGATGCTTAGCGCCTCCCCG	Phytochromes B and D	AT2G18790.1 AT4G16250.1 AT4G18130.1	
PKR	LC2	yes	Robust	yes	yes	TTGATGCTTAGCGCCTCCCCG	Phytochromes B and D	AT2G18790.1 AT4G16250.1 AT4G18130.1	
PKR	LC3	yes	Robust	yes	yes	TTGATGCTTAGCGCCTCCCCG	Phytochromes B and D	AT2G18790.1 AT4G16250.1 AT4G18130.1	
	LC4	no							
	LC5	yes	Not confirmed						
PKR	LC6	yes	Robust	yes	yes	TTGATGCTTAGCGCCTCCCCG	Phytochromes B and D	AT2G18790.1 AT4G16250.1 AT4G18130.1	
	LC7	no							
	LC8	no							
	LC9	no							
PKR	LC10	yes	Mild	yes	yes	TATGACCGAATTTAAAGCCAC	amiRNA-Kinases previously isolated	AT1G73450 AT1G73460 AT3G17750	
PKR	LC11	yes	Mild	yes	yes	TATGACCGAATTTAAAGCCAC	amiRNA-Kinases previously isolated	AT1G73450 AT1G73460 AT3G17750	
	LC12	yes	Not confirmed						
	LC13	yes	Not confirmed						
	LC14	yes	Not confirmed						
PKR	LC15	yes	Mild	yes	yes	TATGACCGAATTTAAAGCCAC	amiRNA-Kinases previously isolated	AT1G73450 AT1G73460 AT3G17750	
PKR	LC16	yes	Mild	yes	yes	TATGACCGAATTTAAAGCCAC	amiRNA-Kinases previously isolated	AT1G73450 AT1G73460 AT3G17750	
PKR / HEC	LC17	yes	Mild	yes	yes	TCAAGAGCGGCACTCGGACTG	Receptor-like protein kinase related	AT3G21910 AT3G21940 AT3G21960 AT3G22010	Lines Growing
	LC18	yes	Not confirmed						
	LC19	no							
	LC20	yes	Not confirmed						
	LC21	yes	Robust	Ongoing					
CSI	LC22	yes	Robust	yes	yes	TCCAAACAGTGGCGCGATCTA	Formin homolog	AT3G05470 AT5G67470	
	LC23	yes	Not confirmed						
CSI	LC24	yes	Mild	yes	yes	TTATCATTTGATAGATTGCTG	F-box protein	AT3G58960 AT4G22280	
UNC / CSI	LC25	yes	Mild	yes	yes	TAAGACACGGCAATTTCGCTA	F-box protein	AT3G54160 AT5G15620	
	LC26	no							
CSI	LC27	yes	Robust	yes	yes	TGTAAATGTTCAAGGTTCCGA	Leucine-rich repeat family protein	AT3G43740.1 AT3G43740.2 AT5G21090.1	Lines Growing
CSI / UNC	LC28	yes	Mild	yes	yes	TATTTAGGTGGTAAGTTCCAG	Nascent polypeptide-associated complex subunit alpha-like protein	AT3G12390 AT5G13850	
	LC29	yes	Not confirmed						
CSI	LC30	yes	Mild	yes	yes	TGTAAATGTTCAAGGTTCCGA	Leucine-rich repeat family protein	AT3G43740.1 AT3G43740.2 AT5G21090.1	Lines Growing
	LC31	no							
	LC32	yes	Not confirmed						

Table 1 Continued:

CSI	LC33	yes	Mild	yes	yes	TGTAAATGTTCAAGGTTCCGA	Leucine-rich repeat family protein	AT3G43740.1 AT3G43740.2 AT5G21090.1	Lines Growing
	LC34	yes	Mild	Ongoing					
TFB	LC35	yes	Mild	yes	yes	TTCAACATGCCAGGCAAACAT	Transcription factor jumonji (jmj) family protein / zinc finger (C5HC2 type) family protein	AT3G48430 AT5G04240 AT5G46910	Lines Growing
	LC36	no							
	LC37	no							
	LC38	yes	Not confirmed						
TFB	LC39	yes	Mild	yes	yes	TCTCTCGCGTTTATAAGCCAA	BEL1-like homeodomain	AT1G19700 AT1G75410 AT2G35940	
CSI	LC40	yes	Mild	yes	yes	TAATGTCGCACCTTTTAGCAC	F-box protein	AT1G30200.1 AT5G46170.1	
CSI / UNC	LC41	yes	Mild	yes	yes	TGAGTAATCATAAATGGCCTC	F-box protein	AT1G66290 AT1G66300 AT1G66310 AT1G66320 AT1G66640 AT1G78750 AT1G78840 AT4G13985	
CSI	LC42	yes	Robust	yes	yes	TAAGCGCATCGAGATCGGCAC	Ribosomal protein S19 family protein	AT1G33850 AT5G09490 AT5G09510 AT5G43640	
CSI	LC43	yes	Mild	yes	yes	TGGAACGGACTCTTACCACGT	Ribosomal protein S26e family protein	AT2G40590 AT3G56340	
	LC44	yes	Not confirmed						
	LC45	yes	Not confirmed						
	LC46	yes	Mild	Ongoing					
	LC47	yes	Robust	Ongoing					
?	LC48	yes	Mild	yes	yes	TCATCGAGGTTTTGAGGCTG	Sec14p-like phosphatidylinositol transfer family protein	AT3G23960.1 AT1G19650.2 AT1G19650.1 AT1G19650.3 AT1G70500.1 AT1G61060.1 AT1G33010.1	
	LC49	yes	Not confirmed						
?	LC50	yes	Robust	yes	yes	TCATCGAGGTTTTGAGGCTG	Sec14p-like phosphatidylinositol transfer family protein	AT3G23960.1 AT1G19650.2 AT1G19650.1 AT1G19650.3 AT1G70500.1 AT1G61060.1 AT1G33010.1	
PEC	LC51	yes	Robust	yes	yes	TATGTATAAGAACTGTTGCAC	tRNAse Z4	AT1G52160 AT3G16260	
	LC52	no							
6-13	LC53	yes	Robust	Ongoing					
PEC	LC54	yes	Robust	yes	yes	TCTTAACGATCCATGAGGCAA	NAD(P)-binding Rossmann-fold superfamily protein	AT1G15950 AT1G51410 AT1G66800 AT1G80820	

Table 1: Continued.

	LC55	no						
TFB	LC56	yes	Mild	yes	yes	TTCAACATGCCAGGCAAACAT	Transcription factor jumonji (jmj) family protein / zinc finger (C5HC2 type) family protein	AT3G48430 AT5G04240 AT5G46910
UNC	LC57	yes	Robust	yes	yes	TTTGGAGGACGTTCTCGCCTA	TRAF-like family protein	AT3G20360 AT3G46190
	LC58	no						
	LC59	no						
7-12	LC60	yes	Mild	Ongoing				
7-12	LC61	yes	Mild	Ongoing				
	LC62	no						
7-12	LC63	yes	Mild	Ongoing				
	LC64	no						
7-3	LC65	yes	Mild	Ongoing				
	LC66	no						
	LC67	no						
	LC68	no						
7-3	LC69	yes	Mild	Ongoing				
8-5	LC70	no						
DMF	LC71	yes	Mild	yes	yes	TAAAGAAGAGCACTTGTACAA	Phototropic-responsive NPH3 family protein	AT1G30440 AT4G37590
UNC	LC72	yes	Mild	yes	yes	TATACATGTCTACGGGAGCTC	Tetratricopeptide repeat (TPR)-like superfamily protein	AT1G04840 AT1G31430
8-5	LC73	yes	Mild	yes	yes	T-TTGGGTTGT-ATGAG--CAG		
8-5	LC74	yes	Mild	Ongoing				
8-9	LC75	yes	Mild	Ongoing				

Table 2: Primer library designed for amiRNA amplification for sequencing and BP reactions for cloning.

Name	Sequence (5' to 3')	S or AS	Gene	Tm	Description
LRR1 RT FP	tcaccgggaaaatcccatcttct	Sense	At3g43740	63	Primer used combined with KJS002. Amplicon size = 155
LRR1 RT RP	tgttccacacaaatcattccctgag	Anti-sense	At3g43740	63	Primer used combined with KJS001. Amplicon size = 155
LRR2 RT FP	tgaccggtccaatccctagagc	Sense	At5g21090	65	Primer used combined with KJS004. Amplicon size = 212
LRR2 RT RP	gttttgccagttgtttcaggtgcag	Anti-sense	At5g21090	65	Primer used combined with KJS003. Amplicon size = 212
JMJ1 RT FP	gcacgcagatattgcagtggtg	Sense	At5g46910	64	Primer used combined with KJS006. Amplicon size = 285
JMJ1 RT RP	atgccaggcaaacatactgaaaagc	Anti-sense	At5g46910	64	Primer used combined with KJS005. Amplicon size = 285
JMJ2 RT FP	tcgggcagccatgaattatctaccc	Sense	At5g04240	66	Primer used combined with KJS008. Amplicon size = 277
JMJ2 RT RP	gtgcgctatgacgcggaagtaaatc	Anti-sense	At5g04240	66	Primer used combined with KJS007. Amplicon size = 277
LRR amiRNA I	gaTGTGTTCTTACAAGGTCACGCtctctcttttgtattcc	Sense	amiRNA		From WMD3 website. To clone TGTGTTCTTACAAGGTCACGC amiRNA.
LRR amiRNA II	gaGCGTGACCTTGTAAGAACACAtcaaagagaatcaatga	Anti-sense	amiRNA		From WMD3 website. To clone TGTGTTCTTACAAGGTCACGC amiRNA.
LRR amiRNA III	gaGCATGACCTTGTATGAACACTtcacaggtcgtgatatg	Sense	amiRNA		From WMD3 website. To clone TGTGTTCTTACAAGGTCACGC amiRNA.
LRR amiRNA IV	gaAGTGTTCATACAAGGTCATGCtctacatatatattcct	Anti-sense	amiRNA		From WMD3 website. To clone TGTGTTCTTACAAGGTCACGC amiRNA.
JMJ amiRNA I	gaTAAAACCGTGGCTGGAAGCAGtctctcttttgtattcc	Sense	amiRNA		From WMD3 website. To clone TAAAACCGTGGCTGGAAGCAG amiRNA.
JMJ amiRNA II	gaCTGCTTCCAGCCACGGTTTTAtcaaagagaatcaatga	Anti-sense	amiRNA		From WMD3 website. To clone TAAAACCGTGGCTGGAAGCAG amiRNA.
JMJ amiRNA III	gaCTACTTCCAGCCAGGGTTTTTtcacaggtcgtgatatg	Sense	amiRNA		From WMD3 website. To clone TAAAACCGTGGCTGGAAGCAG amiRNA.
JMJ amiRNA IV	gaAAAAACCCTGGCTGGAAGTAGtctacatatatattcct	Anti-sense	amiRNA		From WMD3 website. To clone TAAAACCGTGGCTGGAAGCAG amiRNA.
LRR1 attB1	ggggacaagtttgtacaaaaaagcaggcttcaccATGGTGGCGCAAAACAGTCG	Sense	AT3G43740	58	BP reaction
LRR1 attB2 w/o STOP	ggggaccactttgtacaagaaagctgggtaAGTGCAATTGGTGTCATAGCTC	Anti-sense	AT3G43740	55	BP reaction
LRR1 attB2r	ggggacagctttcttgtacaaagtggccATGGTGGCGCAAAACAGTCG	Sense	AT3G43740	58	BP reaction
LRR1 attB3 w/ STOP	GGGGACAACTTTGTATAATAAAGTTGATTAAGTGCAATTGGTGTCATAGCTC	Anti-sense	AT3G43740	55	BP reaction
JMJ1 attB1	ggggacaagtttgtacaaaaaagcaggcttcaccATGGCGGAAAGGAGGATCTG	Sense	At5g46910	56	BP reaction
JMJ1 attB2 w/o STOP	ggggaccactttgtacaagaaagctgggtaCGGCTTTATTAGCCCTTTCAC	Anti-sense	At5g46910	54	BP reaction
JMJ1 attB2r	ggggacagctttcttgtacaaagtggccATGGCGGAAAGGAGGATCTG	Sense	At5g46910	56	BP reaction
JMJ1 attB3 w/ STOP	GGGGACAACTTTGTATAATAAAGTTGATTACGGCTTTATTAGCCCTTTCAC	Anti-sense	At5g46910	55	BP reaction
LLR2 attB1	ggggacaagtttgtacaaaaaagcaggcttcaccATGGCGTCTCGAAACTATCGG	Sense	AT5G21090	56	BP reaction
LLR2 attB2 w/o STOP	ggggaccactttgtacaagaaagctgggtaGGTGCAGTTAGTGTCGTAGC	Anti-sense	AT5G21090	55	BP reaction
LLR2 attB2r	ggggacagctttcttgtacaaagtggccATGGCGTCTCGAAACTATCGG	Sense	AT5G21090	56	BP reaction
LLR2 attB3 w/ STOP	GGGGACAACTTTGTATAATAAAGTTGATCAGGTGCAGTTAGTGTCG	Anti-sense	AT5G21090	55	BP reaction

2.4 Choosing a candidate of interest

While all of these candidates will be characterized in the future, I narrowed my focus on a candidate of interest to characterize with further experiments. LC27, LC30, and LC33 were sequenced and found to contain the same amiRNA insert, TGTAAATGTTCAAGGTTCCGA, which targets the loci AT5G21090 & AT3G43740 (Table 1). Neither of these loci had been characterized previously. AT5G21090 & AT3G43740 are leucine-rich repeat (LRR) family protein genes (Table 1). This candidate was chosen because it was identified three times in the low CO_2 screen (Table 1).

LC10, LC11, LC15, and LC16 were also robust candidates, containing the same amiRNA insert and found to target 3 kinase loci, identified through our screen. This candidate amiRNA has been previously identified by another screen in our lab which validates the success of this screen. Characterization of this amiRNA kinase by Dr. Guillaume Dubeaux is ongoing (Figure 5).

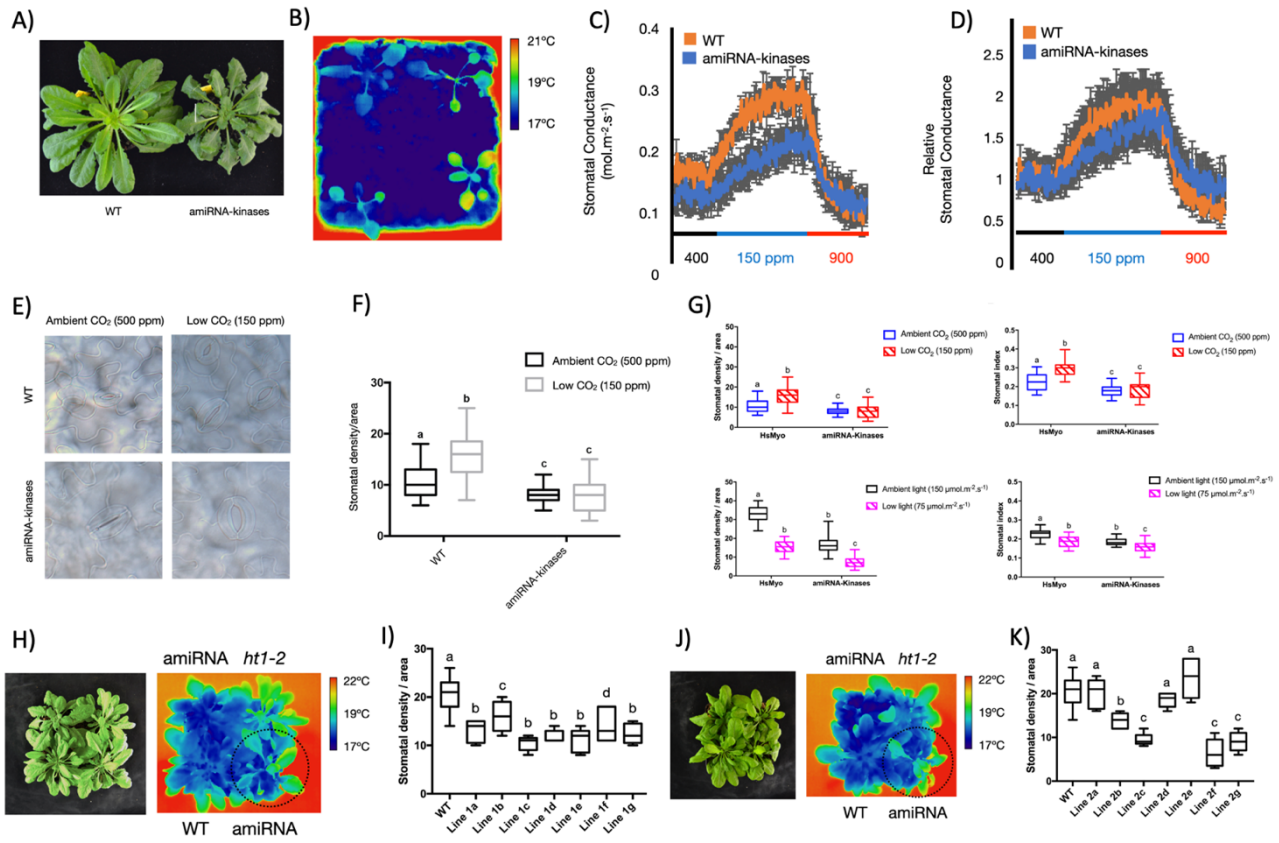

Figure 5: Characterization of amiRNA kinase candidates. Experiments conducted by Dr. Guillaume Dubeaux.

LC10, LC11, LC15, and LC16 were identified in the CO_2 screen. These candidates contain an amiRNA targeting three putative kinases. A) The amiRNA-kinase line has a macroscopic rosette phenotype. B) IR images taken at the T3 generation confirm the canopy leaf temperature phenotype (top left WT HsMYO; top right amiRNA line; bottom left amiRNA line; bottom right *ht1-2* control). C) The amiRNA-kinase line has a WT-like stomatal conductance response during a variable [CO_2] time-resolved gas exchange program. Raw data is shown. D) The amiRNA-kinase line has a WT-like stomatal conductance response during a variable [CO_2] time-resolved gas exchange program. Normalized data is shown. E) The amiRNA-kinase line was imaged via DIC microscopy at ambient and low CO_2 conditions compared to WT HsMYO. F) The amiRNA-kinase line seems insensitive to CO_2-controlled stomatal development. G) The amiRNA-kinase line seems to be sensitive to light-induced stomatal development. H-K) Independent insertions of the same amiRNA sequence shows the same phenotype, validated in IR images and stomatal index/density assay.

2.5 Preliminary characterization of candidates: time-resolved gas exchange analysis of candidate plants showed various conductance phenotypes

The aim of the gas exchange experiment is to characterize the artificial miRNA leucine-rich repeat (LRR) candidate plant, identified from the complementary forward genetic screen, in the context of stomatal conductance response to CO_2 concentration shifts. Using whole, intact *A. thaliana* leaves, gas exchange analyses were performed to study the stomatal conductance response to [CO_2] shifts in the artificial miRNA leucine-rich repeat knockdown candidate (LRR) using amiRNA-HsMYO as the control. Figure 6 shows the gas exchange data for the candidate (LRR), identified by a homologous gene silencing artificial miRNA (amiRNA) screen. The gas exchange program exposes whole intact leaves to different concentrations of CO_2 (ppm) over time, producing a stomatal conductance curve. More gas exchange indicates that the stomatal pores are open, while less exchange means they are closed. In this gas exchange analysis, the wild-type plants open their stomata in response to low CO_2 and shut the pores abruptly when exposed to high CO_2. The data suggests that candidate LRR's stomata open slower and less overall in response to low CO_2 compared to wild-type (Figure 6). In addition, LRR does not shut its stomata as rapidly or abruptly, compared to wild-type, in response to high CO_2 (Figure 6). Compared to wild-type, these data indicate that the amiRNA knockdown candidate LRR has a partially impaired stomatal opening and closure mechanism in response to [CO_2] shifts, suggesting that the knockdown has affected stomatal movements or stomatal development (Figure 6).

Time-resolved gas exchange analyses of the amiRNA candidate LC17 line showed that there was not much of a difference between the stomatal conductance of LC17 and HsMYO in both stomatal opening and closure (Figure 7). There seems to be a slightly different opening slope where LC17 was more linear than HsMYO, and in terms of closure, LC17 seems to continue to

close or maintain closure after exposure to high CO_2 compared to HsMYO. However, these observations are minor, especially because they are well within the standard error of the mean (n=5±SEM) (Figure 7A). Normalized conductance data showed that LC17 closely resembles HsMYO in stomatal opening and closure (Figure 7B).

Time-resolved gas exchange analyses of the amiRNA candidate LC24 line showed that, compared to HsMYO, there was not much of a difference between the stomatal conductance of LC24 and HsMYO in both stomatal opening and closure (Figure 8). There seems to be a slightly different opening slope where LC24 was more linear than HsMYO, and in terms of closure, LC24 seems to resemble HsMYO (Figure 8A). Normalized conductance data showed that LC24 has a linear slope of stomatal opening compared to HsMYO (Figure 8B).

Time-resolved gas exchange analyses of the amiRNA candidate LC28 line showed that, compared to HsMYO, LC28's stomata open slower, and to a lesser extent, in response to low CO_2 compared to wild-type (Figure 9). However, LC28 has similar stomatal closing to wild-type, in response to high CO_2 (Figure 9). These data, compared to wild-type, indicate that the amiRNA knockdown candidate LC28 has a partially impaired stomatal opening and closure mechanism in response to [CO_2] shifts, suggesting that the knockdown has affected stomatal movements or stomatal development (Figure 9A). Normalized conductance data showed that LC28 has impaired stomatal opening but similar closure to HsMYO (Figure 9B).

Time-resolved gas exchange analyses of the amiRNA candidate LC35 line showed that, compared to HsMYO, there was a marked difference between the stomatal conductance of LC35 and HsMYO in both stomatal opening and closure (Figure 10). LC35 has an impaired opening and closure response compared to HsMYO, with linear slopes in stomatal conductance for both (Figure

10A). Normalized conductance data showed that LC35 does not open as much or at the same rate as HsMYO (Figure 10B). The stomatal closure of LC35 was not as fast as HsMYO (Figure 10B).

Time-resolved gas exchange analyses of the amiRNA candidate LC10 line showed that, compared to HsMYO, there was a large difference between the stomatal conductance of LC10 and HsMYO in both stomatal opening and closure (Figure 11). Normalized conductance data showed that LC10 is impaired in stomatal opening in response to low CO_2 compared to HsMYO; the candidate does not open at the same rate or at the same level as HsMYO (Figure 11B). LC10 also has impaired stomatal closure compared to HsMYO; the candidate's stomatal closure is as fast as HsMYO, but does not fully close (Figure 11B).

Time-resolved gas exchange analyses of the amiRNA candidate LC56 line showed that, compared to HsMYO, there a significant difference between the stomatal conductance of LC56 and HsMYO in both stomatal opening and closure (Figure 12). Normalized conductance data showed that LC56 is drastically impaired in stomatal opening in response to low CO_2 compared to HsMYO; the candidate hardly opened at both the rate or at the same level as HsMYO (Figure 12B). LC56 also seemed to have impaired stomatal closure compared to HsMYO, but is difficult to determine because there was not much opening to begin with (Figure 12B).

Time-resolved gas exchange analyses of the FOX candidate LF3 line showed that, compared to Col-0, there was a difference between the stomatal conductance of LF3 and Col-0 in stomatal opening, but not closure (Figure 13). LF3 has an impaired stomatal opening response compared to Col-0, but stomatal closure response closely resembles the control (Figure 13).

Time-resolved gas exchange analyses of the FOX candidate LF7 line showed that, compared to Col-0, there was a difference between the stomatal conductance of LF7 and Col-0 in

stomatal opening, but not closure (Figure 14). LF7 has an impaired stomatal opening response compared to Col-0, but stomatal closure response closely resembles the control (Figure 14).

More gas exchange analyses are ongoing for these candidates. KO mutants will be isolated to confirm the obtained results.

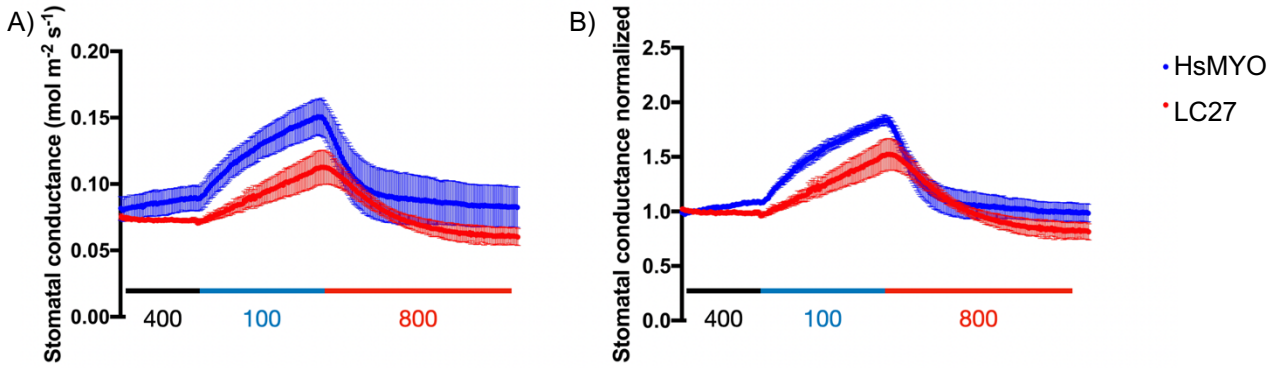

Figure 6: Whole-leaf gas exchange recording of the artificial miRNA knockdown candidate (LC27), identified by loss-of-function screen, compared to the amiRNA-HsMYO control.

Gas exchange analysis was performed to study the *A. thaliana* amiRNA knockdown candidate LRR (LC27) stomatal conductance response to [CO_2] shifts compared to HsMYO. The stomatal conductance of HsMYO and LRR was analyzed using the gas exchange analyzer, LiCOR 6400XT. Each leaf was equilibrated at ambient [CO_2]=400 ppm for one hour prior to recording. The [CO_2] in ppm over time for the LiCOR 6400XT program is indicated on the x-axis, while the stomatal conductance ($mol \cdot m^{-2}s^{-1}$) is shown on the y-axis. These data were gathered from five leaves of five independent 8-week-old plants and represent the normalized average of n=5±SEM leaves per genotype. A) The raw data gas exchange recording shows the stomatal conductance of the candidate compared to HsMYO. B) The stomatal conductance over time was normalized for the leaf area.

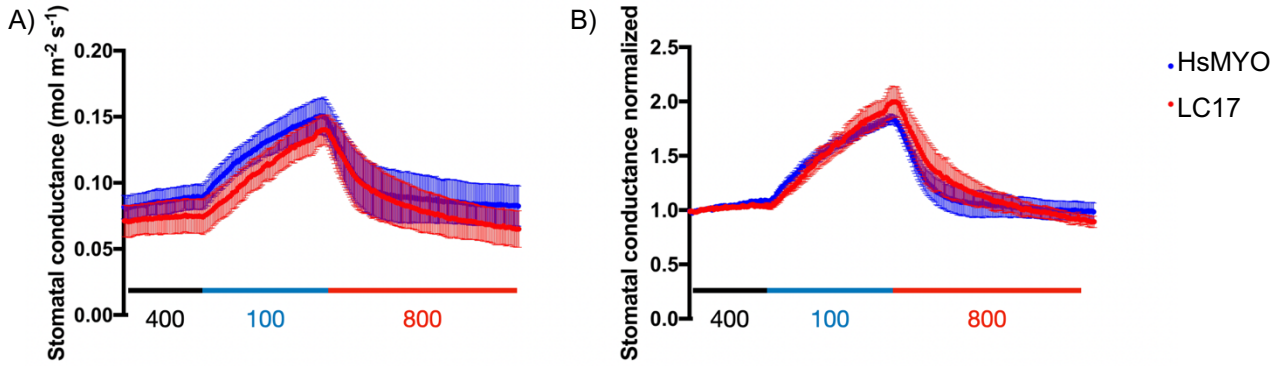

Figure 7: Candidate LC17 response to [CO_2] shifts over time.

The stomatal conductance of HsMYO and LC17 was analyzed using the gas exchange analyzer, LiCOR 6400XT. Each leaf was equilibrated at ambient [CO_2]=400 ppm for one hour prior to recording. The [CO_2] in ppm over time for the LiCOR 6400XT program is indicated on the x-axis, while the stomatal conductance ($mol \cdot m^{-2}s^{-1}$) is shown on the y-axis. These data were gathered from five leaves of five independent 8-week-old plants and represent the normalized average of n=5±SEM leaves per genotype. A) The raw data gas exchange recording shows the stomatal conductance of the candidate compared to HsMYO. B) The stomatal conductance over time was normalized for the leaf area.

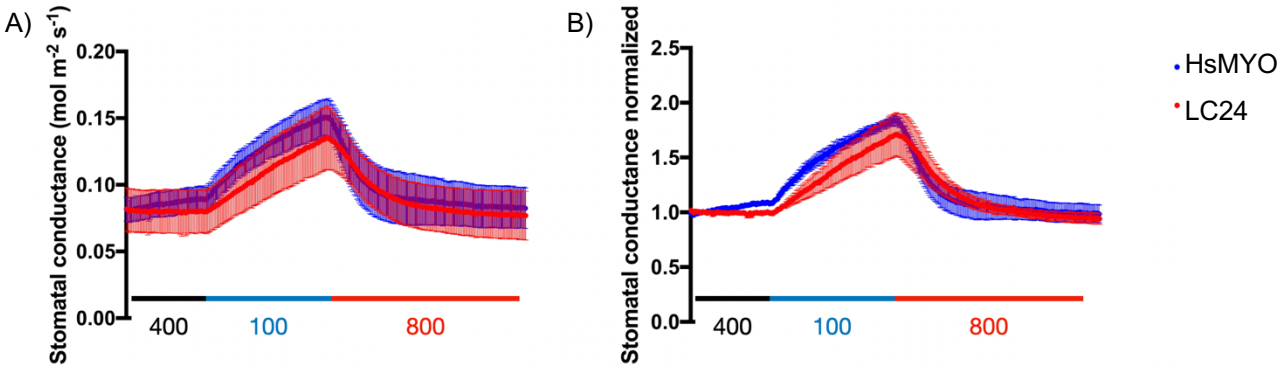

Figure 8: Candidate LC24 response to [CO_2] shifts over time.

The stomatal conductance of HsMYO and LC24 was analyzed using the gas exchange analyzer, LiCOR 6400XT. Each leaf was equilibrated at ambient [CO_2]=400 ppm for one hour prior to recording. The [CO_2] in ppm over time for the LiCOR 6400XT program is indicated on the x-axis, while the stomatal conductance ($mol \cdot m^{-2}s^{-1}$) is shown on the y-axis. These data were gathered from five leaves of five independent 8-week-old plants and represent the normalized average of n=5±SEM leaves per genotype. A) The raw data gas exchange recording shows the stomatal conductance of the candidate compared to HsMYO. B) The stomatal conductance over time was normalized for the leaf area.

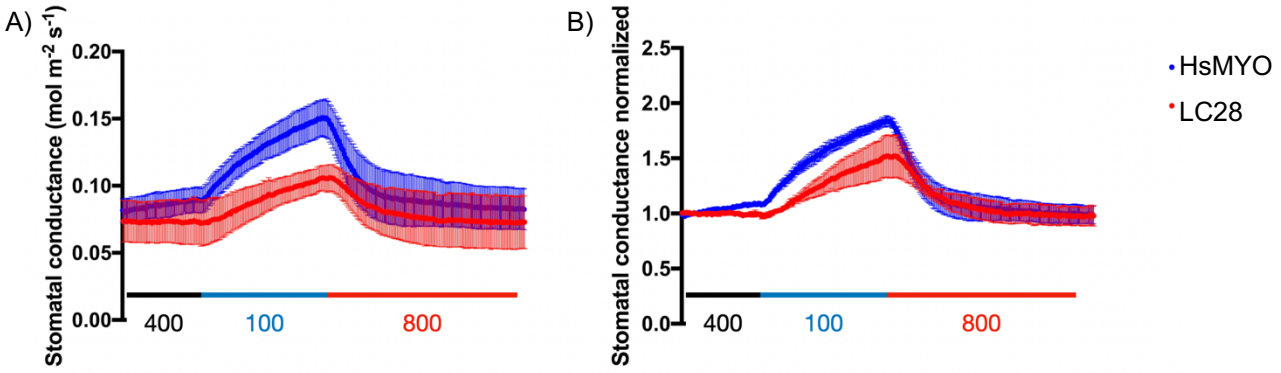

Figure 9: Candidate LC28 response to [CO_2] shifts over time.

The stomatal conductance of HsMYO and LC28 was analyzed using the gas exchange analyzer, LiCOR 6400XT. Each leaf was equilibrated at ambient [CO_2]=400 ppm for one hour prior to recording. The [CO_2] in ppm over time for the LiCOR 6400XT program is indicated on the x-axis, while the stomatal conductance ($mol \cdot m^{-2}s^{-1}$) is shown on the y-axis. These data were gathered from five leaves of five independent 8-week-old plants and represent the normalized average of n=5±SEM leaves per genotype. A) The raw data gas exchange recording shows the stomatal conductance of the candidate compared to HsMYO. B) The stomatal conductance over time was normalized for the leaf area.

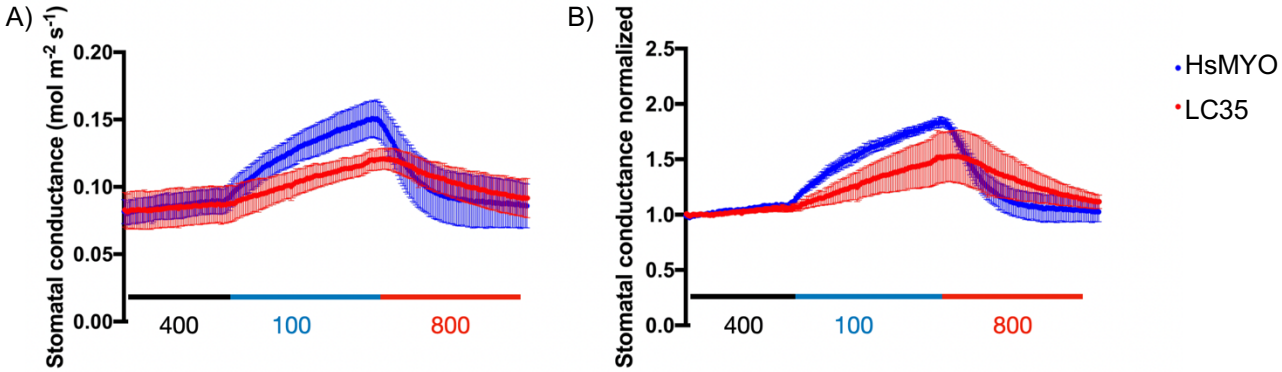

Figure 10: Candidate LC35 response to [CO_2] shifts over time.

The stomatal conductance of HsMYO and LC35 was analyzed using the gas exchange analyzer, LiCOR 6400XT. Each leaf was equilibrated at ambient [CO_2]=400 ppm for one hour prior to recording. The [CO_2] in ppm over time for the LiCOR 6400XT program is indicated on the x-axis, while the stomatal conductance ($mol \cdot m^{-2}s^{-1}$) is shown on the y-axis. These data were gathered from five leaves of five independent 8-week-old plants and represent the normalized average of n=5±SEM leaves per genotype. A) The raw data gas exchange recording shows the stomatal conductance of the candidate compared to HsMYO. B) The stomatal conductance over time was normalized for the leaf area.

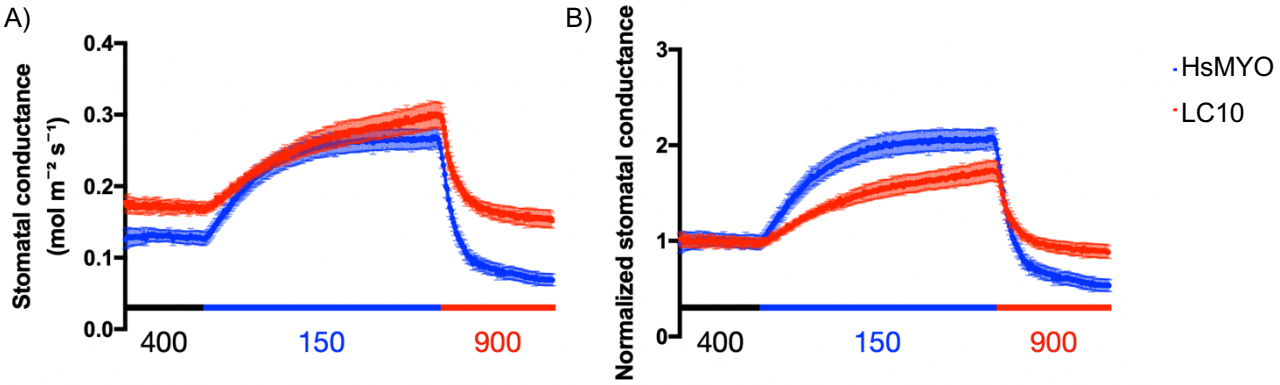

Figure 11: Candidate LC10 response to [CO_2] shifts over time.

The stomatal conductance of HsMYO and LC10 was analyzed using the gas exchange analyzer, LiCOR 6400XT. Each leaf was equilibrated at ambient [CO_2]=400 ppm for one hour prior to recording. The [CO_2] in ppm over time for the LiCOR 6400XT program is indicated on the x-axis, while the stomatal conductance (mol·$m^{-2}s^{-1}$) is shown on the y-axis. These data were gathered from five leaves of five independent 8-week-old plants and represent the normalized average of n=5±SEM leaves per genotype. A) The raw data gas exchange recording shows the stomatal conductance of the candidate compared to HsMYO. B) The stomatal conductance over time was normalized for the leaf area.

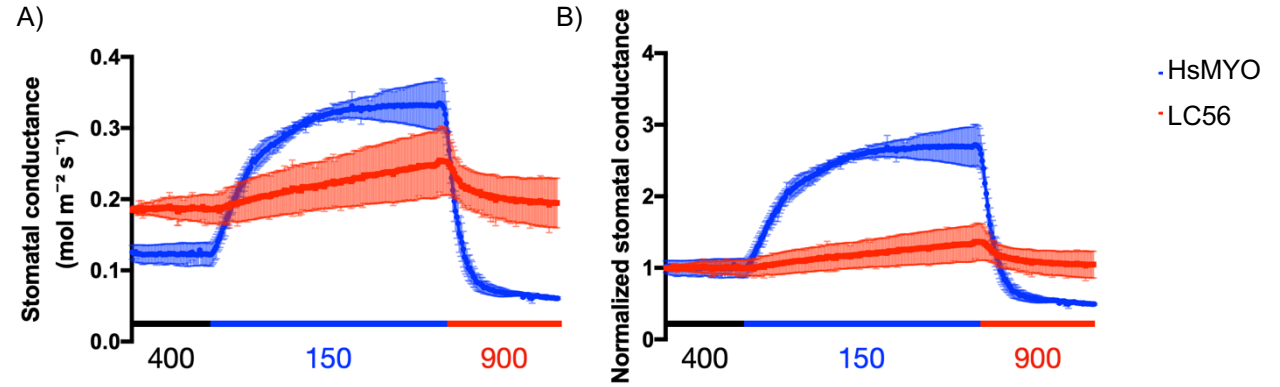

Figure 12: Candidate LC56 response to [CO_2] shifts over time.

The stomatal conductance of HsMYO and LC56 was analyzed using the gas exchange analyzer, LiCOR 6400XT. Each leaf was equilibrated at ambient [CO_2]=400 ppm for one hour prior to recording. The [CO_2] in ppm over time for the LiCOR 6400XT program is indicated on the x-axis, while the stomatal conductance (mol·$m^{-2}s^{-1}$) is shown on the y-axis. These data were gathered from five leaves of five independent 8-week-old plants and represent the normalized average of n=5±SEM leaves per genotype. A) The raw data gas exchange recording shows the stomatal conductance of the candidate compared to HsMYO. B) The stomatal conductance over time was normalized for the leaf area.

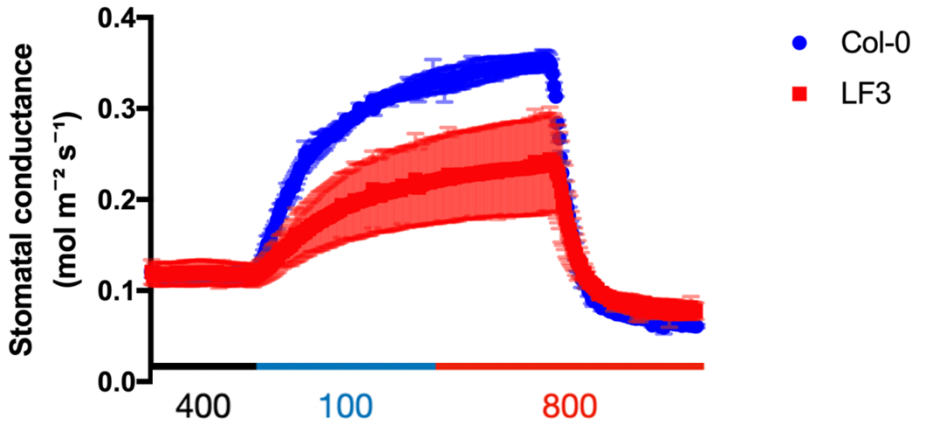

Figure 13: Candidate LF3 response to [CO_2] shifts over time.

The stomatal conductance of HsMYO and LF3 was analyzed using the gas exchange analyzer, LiCOR 6400XT. Each leaf was equilibrated at ambient [CO_2]=400 ppm for one hour prior to recording. The [CO_2] in ppm over time for the LiCOR 6400XT program is indicated on the x-axis, while the stomatal conductance ($mol \cdot m^{-2}s^{-1}$) is shown on the y-axis. These data were gathered from five leaves of five independent 8-week-old plants and represent the normalized average of n=5±SEM leaves per genotype.

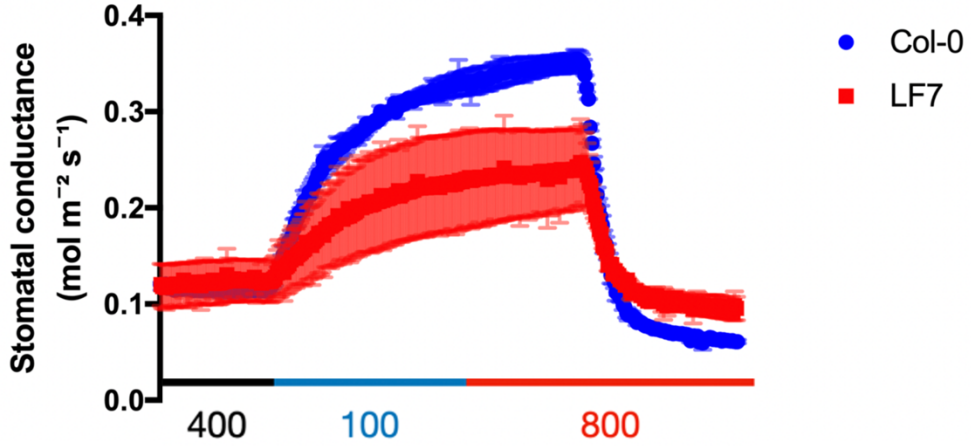

Figure 14: Candidate LF7 response to [CO_2] shifts over time.

The stomatal conductance of HsMYO and LF7 was analyzed using the gas exchange analyzer, LiCOR 6400XT. Each leaf was equilibrated at ambient [CO_2]=400 ppm for one hour prior to recording. The [CO_2] in ppm over time for the LiCOR 6400XT program is indicated on the x-axis, while the stomatal conductance ($mol \cdot m^{-2}s^{-1}$) is shown on the y-axis. These data were gathered from five leaves of five independent 8-week-old plants and represent the normalized average of n=5±SEM leaves per genotype.

2.6 Preliminary characterization of candidates: further investigation of stomatal morphology and development

To determine whether stomatal movement or stomatal development are responsible for the partially impaired stomatal conductance phenotype of LC27 in the gas exchange experiments, further investigation of stomatal morphology and development was conducted.

Double-blind stomatal index and density assays were conducted for amiRNA candidates LC17, LC24, LC27, LC28, LC35, LC42, and LC43 compared to HsMYO (Figures 15-21). LC30, the same amiRNA as LC27, was analyzed again in a second double-blind stomatal index and density assay compared to HsMYO (Figure 22). A third double-blind stomatal index and density assay is ongoing for LC30. A double-blind stomatal size assay is ongoing for LC27/30/33.

The assays were all performed as follows: 5 plants per genotype were grown under 12/12 light dark cycles and the 5th true leaf was harvested at 4-weeks-old. The abaxial side of the leaf was imaged via DIC (differential interference contrast) microscopy. The images were counted via the Cell Counter Image J software. Prism was used to plot the data in box-whisker graphs and run paired two-tailed t-tests with Welch's correction for all candidates.

Figure 17 depicts a double-blind stomatal index and density assay of LC27. Double-blinding was achieved with a team effort: one team member blinded the genotypes, another imaged, and a third counted the cells. The data was unblinded for statistical analysis and data processing. A paired two-tailed t-test with Welch's correction was run yielding $p<0.0001$ and $p<0.0001$ for stomatal index and density, respectively. This is indicated in Figure 17 by three ***, which is a highly significant difference. The stomatal index of LC27 was slightly lower than HsMYO and stomatal density of LC27 was lower than HsMYO (Figure 17).

Figure 22 depicts a second double-blind stomatal index and density assay of LC30, which contains the same amiRNA insert as LC27, but LC30 was used instead because of seed availability. A paired two-tailed t-test with Welch's correction was run yielding $p<0.0001$ and $p<0.0001$ for stomatal index and density, respectively. This is indicated in Figure 22 by three ***, which is a highly significant difference. The stomatal index of LC30 was much lower than HsMYO and stomatal density of LC30 was much lower than HsMYO (Figure 22). This data suggests that LC30 may be implicated in stomatal development.

Microscopy images of the 4-week-old abaxial side of amiRNA candidate 5th-true-leaves were taken at 40X magnification and 1200x1200 resolution (Figure 23). Seven plants per genotype were imaged and five pictures were taken per leaf. Upon close investigation, the candidate LC30 seems to have markedly larger cells, both pavement and stomata, compared to HsMYO (Figure 23). As previously mentioned, a size assay to measure stomatal aperture and height is ongoing for LC27/30/33.

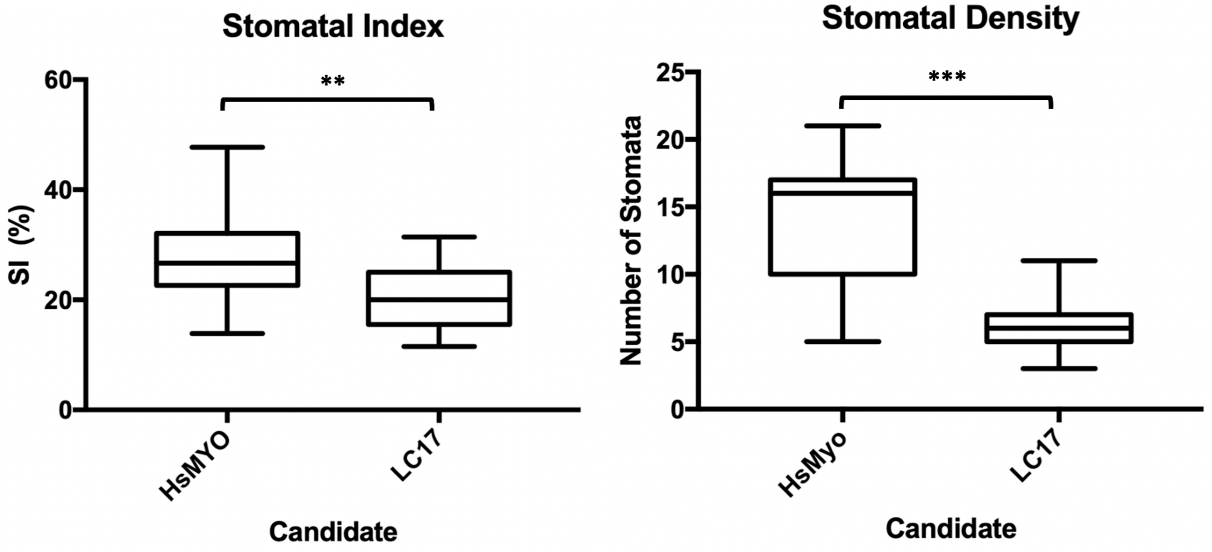

Figure 15: Box plot of double-blind stomatal index (SI %) and density assays conducted using HsMYO and LC17.

Seven plants for each genotype were analyzed. The fifth true leaf of 4-week-old plants were cut and the abaxial side was imaged under a light microscope at 40x magnification, 1200x1200 resolution. For the stomatal index and density data, $p=0.0002$ and $p<0.0001$, respectively, after a paired two-tailed t-test with Welch's correction was conducted.

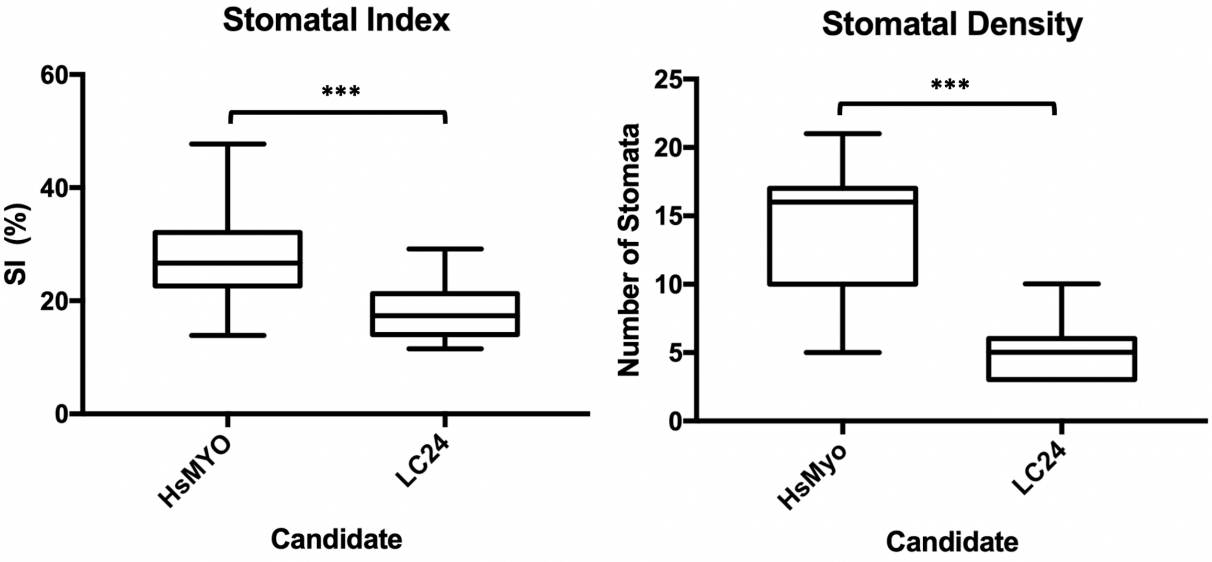

Figure 16: Box plot of double-blind stomatal index (SI %) and density assays conducted using HsMYO and LC24.

Seven plants for each genotype were analyzed. The fifth true leaf of 4-week-old plants were cut and the abaxial side was imaged under a light microscope at 40x magnification, 1200x1200 resolution. For the stomatal index and density data, $p<0.0001$ and $p<0.0001$, respectively, after a paired two-tailed t-test with Welch's correction was conducted.

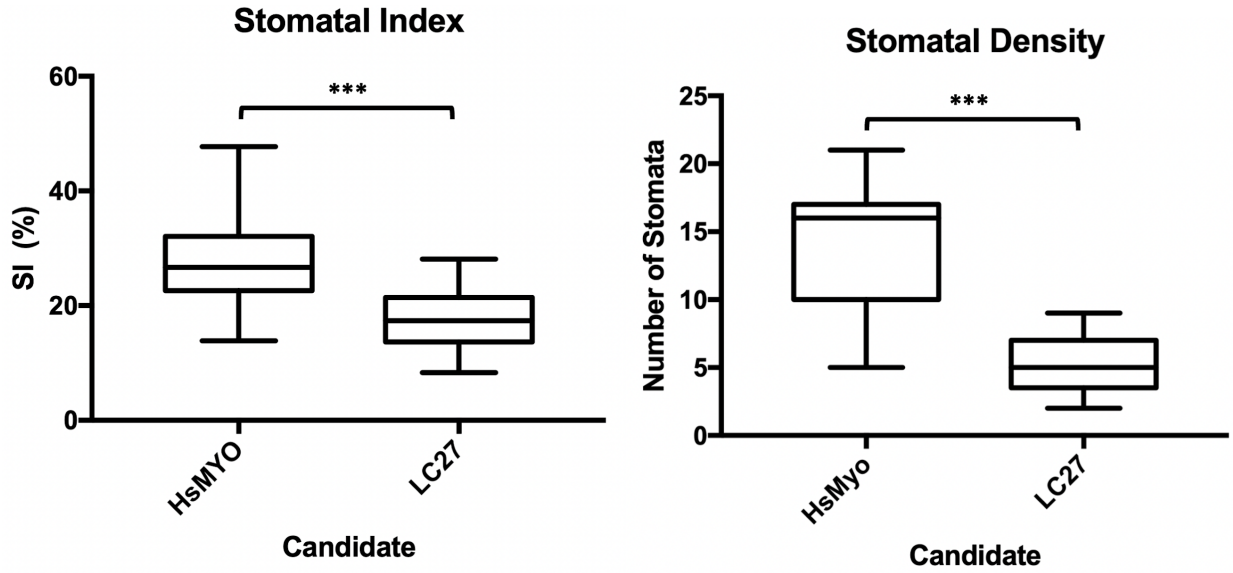

Figure 17: Box plot of double-blind stomatal index (SI %) and density assays conducted using HsMYO and LC27.

Seven plants for each genotype were analyzed. The fifth true leaf of 4-week-old plants were cut and the abaxial side was imaged under a light microscope at 40x magnification, 1200x1200 resolution. For the stomatal index and density data, $p<0.0001$ and $p<0.0001$, respectively, after a paired two-tailed t-test with Welch's correction was conducted.

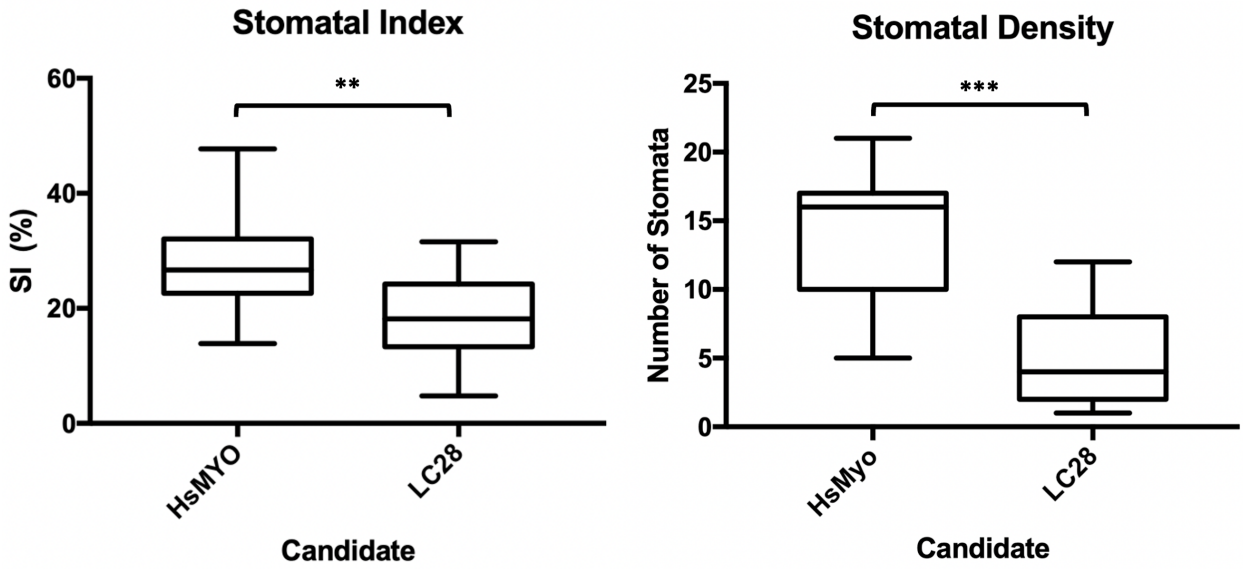

Figure 18: Box plot of double-blind stomatal index (SI %) and density assays conducted using HsMYO and LC28.

Seven plants for each genotype were analyzed. The fifth true leaf of 4-week-old plants were cut and the abaxial side was imaged under a light microscope at 40x magnification, 1200x1200 resolution. For the stomatal index and density data, $p=0.0002$ and $p<0.0001$, respectively, after a paired two-tailed t-test with Welch's correction was conducted.

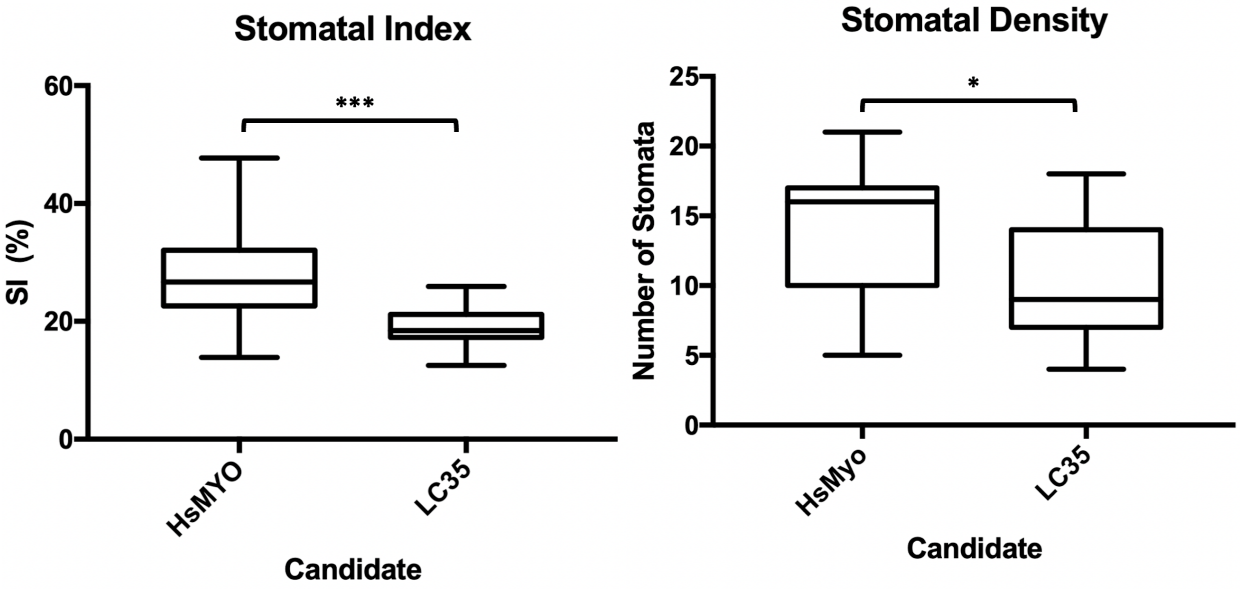

Figure 19: Box plot of double-blind stomatal index (SI %) and density assays conducted using HsMYO and LC35.

Seven plants for each genotype were analyzed. The fifth true leaf of 4-week-old plants were cut and the abaxial side was imaged under a light microscope at 40x magnification, 1200x1200 resolution. For the stomatal index and density data, $p<0.0001$ and $p=0.0091$, respectively, after a paired two-tailed t-test with Welch's correction was conducted.

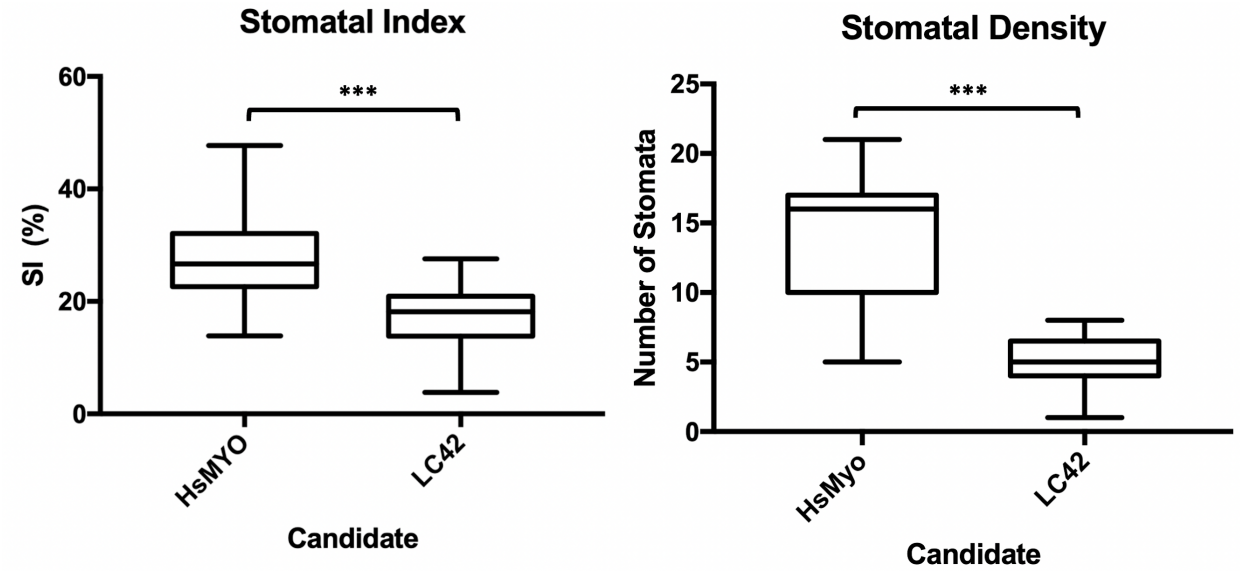

Figure 20: Box plot of double-blind stomatal index (SI %) and density assays conducted using HsMYO and LC42.

Seven plants for each genotype were analyzed. The fifth true leaf of 4-week-old plants were cut and the abaxial side was imaged under a light microscope at 40x magnification, 1200x1200 resolution. For the stomatal index and density data, $p<0.0001$ and $p<0.0001$, respectively, after a paired two-tailed t-test with Welch's correction was conducted.

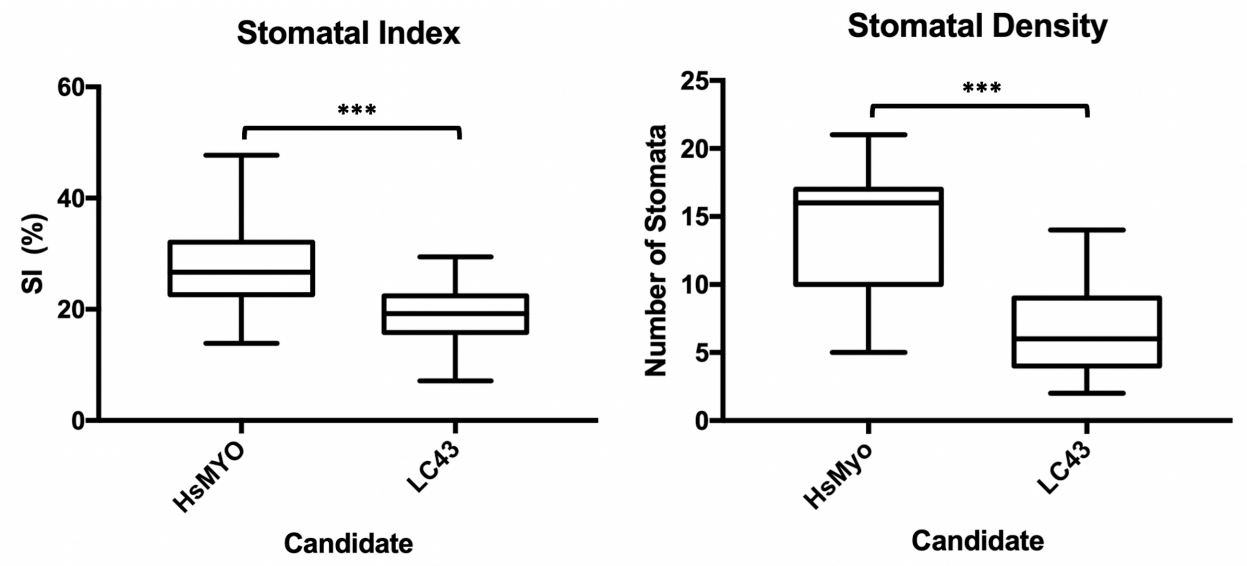

Figure 21: Box plot of double-blind stomatal index (SI %) and density assays conducted using HsMYO and LC43.

Seven plants for each genotype were analyzed. The fifth true leaf of 4-week-old plants were cut and the abaxial side was imaged under a light microscope at 40x magnification, 1200x1200 resolution. For the stomatal index and density data, $p<0.0001$ and $p<0.0001$, respectively, after a paired two-tailed t-test with Welch's correction was conducted.

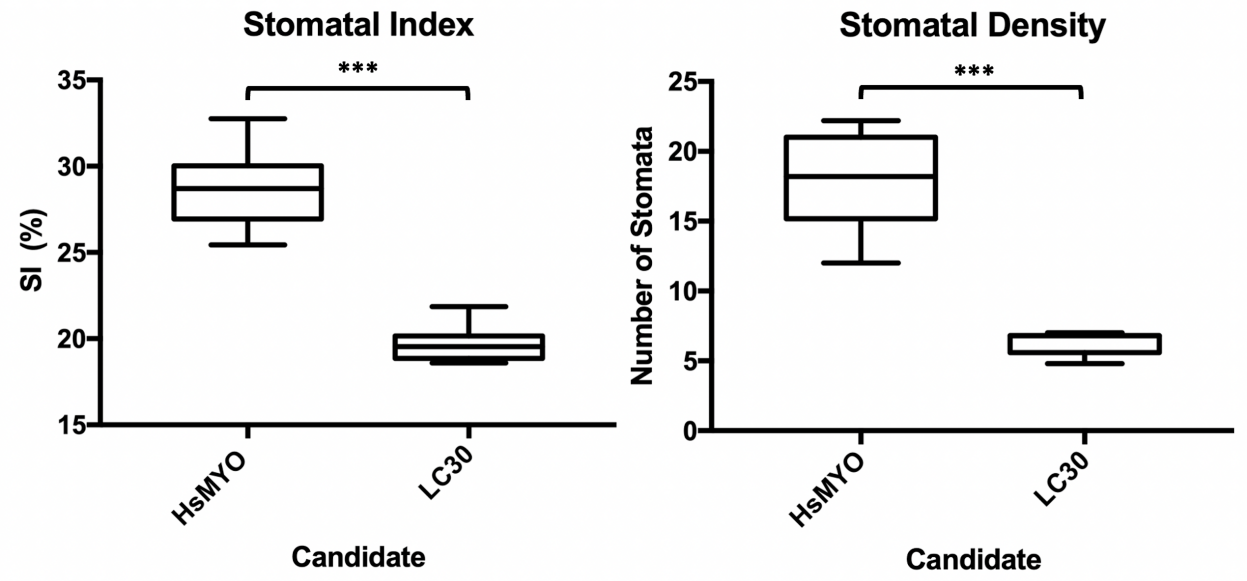

Figure 22: Box plot of double-blind stomatal index (SI %) and density assays conducted using HsMYO and LC30.

Seven plants for each genotype were analyzed. The fifth true leaf of 4-week-old plants were cut and the abaxial side was imaged under a light microscope at 40x magnification, 1200x1200 resolution. For the stomatal index and density data, $p<0.0001$ and $p<0.0001$, respectively, after a paired two-tailed t-test with Welch's correction was conducted.

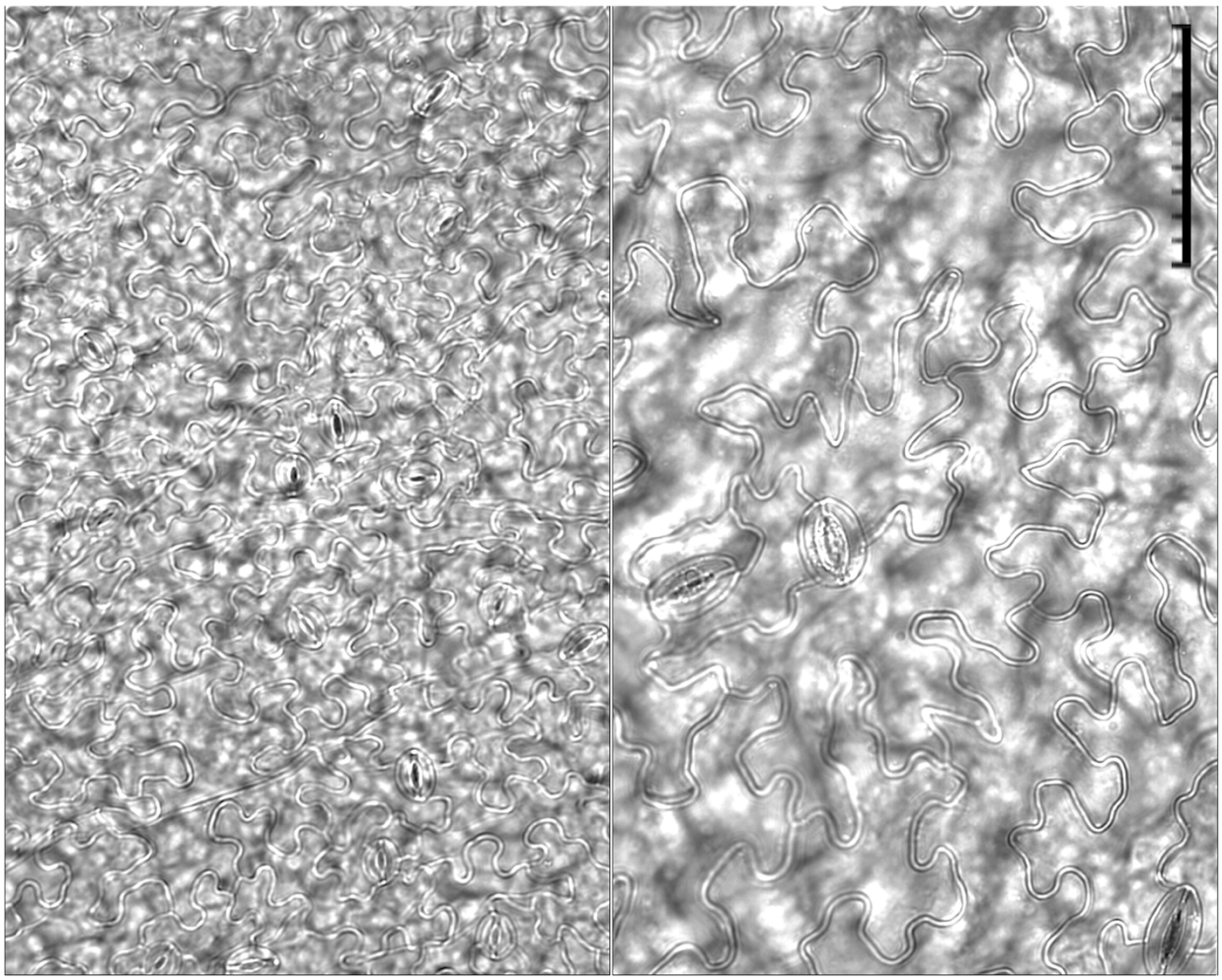

Figure 23: Representative microscopy images of *A. thaliana* leaves from HsMYO and candidate LC30.

Stomatal index and density assay were conducted using HsMYO (left) and LC30 (right) using microscopy images. Seven plants for each genotype were imaged; five pictures taken per leaf. The fifth true leaf of 4-week-old plants were cut and the abaxial side was imaged using a Nikon Eclipse TS100 microscope camera and the Sharpcap 3.1 program at 40x magnification and 1200x1200 resolution. Scale bar represents 0.1mm, with 0.01mm subdivisions.

2.7 Preliminary characterization of candidates: further characterization using published datasets

LC27/30/33 contains an amiRNA targeting two loci: AT5G21090 & AT3G43740. Using ePlant, which uses published datasets, an interactome was generated for one locus (AT3G43740) (Figure 24). There were no known interactors identified for AT5G21090. TAIR identifies the three putative interactors with LRR locus AT3G43740: AT4G02010 as a protein kinase superfamily protein, AT4G27800 as TAP38/PPH1, and AT5G63770 as DGK2.

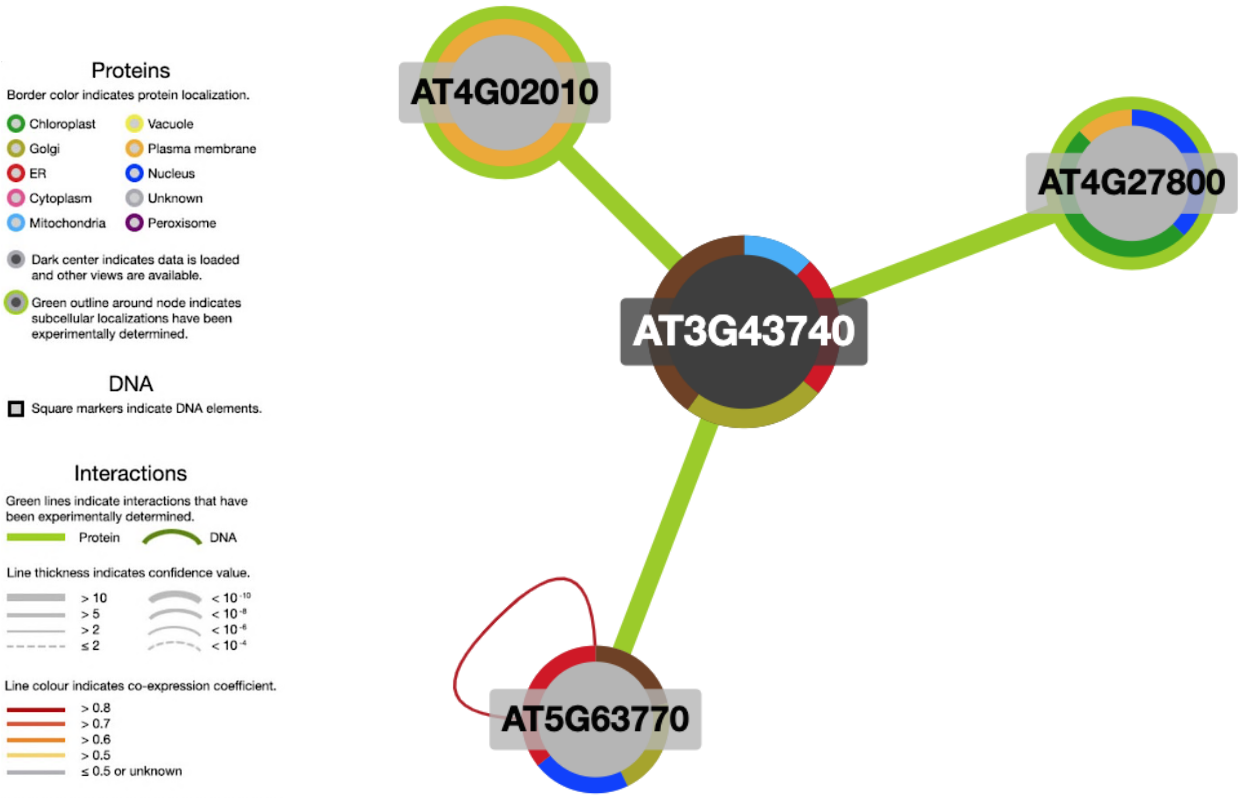

Figure 24: The ePlant Interactome generated for a locus of the candidate of interest, LC27/30/33, which contains an amiRNA targeting loci: AT5G21090 & AT3G43740.

Both LRR family proteins have not been previously characterized. TAIR identifies the interactors (shown above connected to the LRR, **AT3G43740**) AT4G02010 as a protein kinase superfamily protein, AT4G27800 as TAP38/PPH1, and AT5G63770 as DGK2. LRR AT5G21090 did not have any known interactors via ePlant databases.

3. DISCUSSION:

Crop plants make up over two-thirds of the human diet (Nunes et al., 2020; Buckley et al., 2020), making it essential that we understand how rapidly rising global atmospheric CO_2 levels affect plant growth and development. To fully comprehend the effect of CO_2 on plants, it is important to understand how plants respond to CO_2, how they transduce this signal, and what pathways are involved. Stomata, the specialized structures evolved by plants to allow gas exchange with the environment, are found on the epidermis of leaves (Willmer & Fricker, 1996; Peterson et al., 2010). Two kidney-shaped guard cells make up the stomatal complex in dicots, including *Arabidopsis thaliana* (Metcalfe & Chalk, 1950; Van Cotthem, 1970). However, many of the components involved in CO_2 sensing for both stomatal movements and development remain unknown.

3.1 Forward Genetic Screening

To elucidate novel factors involved in the guard cell CO_2 sensing and signaling pathway in plants, a complementary forward genetic screen was conducted in *A. thaliana* using a homologous gene silencing artificial miRNA (amiRNA) approach, and the gain-of-function FOX-hunting system (Hauser et al., 2013; Hauser et al., 2019; Ichikawa et al., 2006). AmiRNA lines, which can be designed to knock down multiple gene targets, were one method used to overcome the functional overlap or genetic redundancy of plant gene families that make forward genetic screens difficult (Ma et al., 2009; Park et al., 2009). The gain-of-function plant line, FOX-hunting, was utilized to overcome this redundancy as well by overexpressing the cDNA to have a drastic and, thus, identifiable phenotype (Ichikawa et al., 2006).

This project was developed to screen large populations for a CO_2-insensitive canopy leaf temperature phenotype. The screen was designed to use both high and low CO_2 incubation prior to infrared (IR) imaging. At high atmospheric [CO_2], WT plants close their stomata and become warmer, while CO_2-insensitive mutants remain cool. At low atmospheric [CO_2], WT plants open their stomata and appear cooler, while CO_2-insensitive mutants would appear warmer. When the screen was conducted with high CO_2, putative cooler CO_2-insensitive candidates were indistinguishable against damp soil. A better background contrast was needed, but dry soil was not an option due to the possibility that drought-induced stomatal movements could be identified instead. Therefore, only low CO_2 incubation was used to screen for CO_2-insensitive canopy leaf temperature phenotype mutants.

Stomatal movement mutants have a mechanical impairment in their opening and/or closure which can be identified through this screen due to their warm canopy leaf temperature when exposed to low CO_2. Stomatal development has also been shown to be affected by CO_2 levels, therefore mutants with a stomatal development phenotype (different number of stomata or different sized stomata) were screened for as well. Stomatal development mutants with fewer stomata appear warmer than WT when exposed to low CO_2, even if all stomata are opening fully because there are not enough open pores to result in leaf cooling (Harrison et al., 2020). Therefore, IR imaging is an excellent tool for indirectly visualizing these stomatal movement or stomatal development phenotypes (Yibing et al., 2004; Merlot et al., 2002).

The amiRNA screen consisted of 14,000 individual T2 amiRNA lines, split into 124 amiRNA pools, with approximately 90 lines per pool, and each line represented by approximately 20 seeds (Hauser et al., 2019). Additionally, 20,496 FOX-hunting lines, split into 410 FOX-

hunting pools, were screened with approximately 50 lines per pool, with each line represented by approximately 8 seeds (Ichikawa et al., 2006).

T2 generation plants were grown at ambient CO_2 (400 ppm) for 3-4 weeks prior to being screened after incubation in low CO_2 conditions, 150 ppm for 2 hours, and then visualized via infrared imaging. Candidates that displayed a warm canopy leaf temperature compared to WT (HsMYO) and *ht1-2* were isolated and collected for validation at the T3 generation. Representative IR images are shown for a putative candidate from amiRNA pool 4 (Figure 1A). Figure 1A shows how putative warm candidates appear in IR imaging compared to WT and *ht1-2*. The putative candidate stands out from the leaf canopy due to its entire rosette being identifiably warmer than the surrounding plants, and resembling the warm leaf control, *ht1-2* (Figure 1A). Upon further temperature analysis using ImageJ, the putative candidate is quantitatively warmer than both the WT and warm (*ht1-2*) controls (Figure 1C).

Validation of the warm phenotype at the T3 generation was done by re-screening the candidates under the same low-CO_2 conditions and IR visualization. Two candidate plants were placed alongside the controls, WT HsMYO and *ht1-2*, in a single pot. The two candidates were considered validated if they were warmer than WT HsMYO. A representative IR image is shown for LC2 (Figure 2A). Directly following 2 hours of low CO_2 incubation, the candidate LC2 was warmer than WT HsMYO, and was nearly as warm as *ht1-2* (Figure 2C). The warm canopy leaf temperature phenotype is not expected to be as strong at the T3 generation because of the silencing of the promoter used in the amiRNA lines, P35S (Rajeevkumar et al., 2015; Amack & Antunes et al., 2020). This promoter is silenced over the generations because it is not endogenous to *A. thaliana* so the plant gradually silences the foreign promoter, leading to variation in expression in the subsequent generations (Rajeevkumar et al., 2015; Amack & Antunes et al., 2020). We see this

in the variable rosette phenotypes in Figures 3 and 4. There is also the possibility of variation due to allelic differences. Plants homozygous for the amiRNA can exhibit a more dramatic phenotype, while a heterozygous candidate may have some functional gene compensation leading to a milder phenotype.

3.2 Characterization

Validated candidates were sequenced (Table 1) and further characterization was pursued, giving us 43 amiRNA and 19 FOX confirmed candidates validated in the T3 generation (Table 1). The majority of the amiRNA candidates were sequenced and the gDNA extraction, amplification, and sequencing of the remaining amiRNA candidates and the 19 FOX mutant candidates is ongoing and will be continued by Dr. Guillaume Dubeaux. Four candidates (LC10, LC11, LC15, and LC16) were identified through the screen as amiRNA-kinases (Table 1; Figure 5). These candidates were previously isolated through another CO_2 screen in our lab which indicates that our screening protocol was able to successfully isolate CO_2-insensitive lines. The amiRNA-kinase lines are currently being characterized by Dr. Guillaume Dubeaux (Figure 5). The data shown in Figure 5 suggest that the amiRNA-kinase candidate seems to be implicated in stomatal development. Another robust candidate, amiRNA candidate LC2 (Figure 2), was identified to be an amiRNA targeting three different phytochromes: PHYB, PHYD, and PHYE (Arabidopsis Genome Initiative, 2000). Phytochromes A-E are far-red/red responsive photoreceptors (Wang et al., 2010; Viczián et al., 2019; Yang et al., 2020). PHYB has been implicated in stomatal movements, specifically by mediating stomatal opening in response to red light (Wang et al., 2010; Viczián et al., 2019; Yang et al., 2020). In addition, there are other photoreceptors implicated in stomatal movements, such as PHOT1 and PHOT2, which induce stomatal opening in response to blue light (Talbott et al., 2003; Yang et al., 2020). Identifying factors that have been implicated in

stomatal movements, such as the PHYB/PHYD/PHYE-targeting amiRNA candidate LC2, indicates that this screen was successful in detecting robust candidates. Overall, this is promising for the plant science community because the complementary screens produced 43 amiRNA and 19 FOX candidate mutants that will be characterized, and it is likely that a factor involved in guard cell CO_2 signaling could be among them.

The most robust, uncharacterized candidates identified from the screen were LC17, LC24, LC27, LC28, LC30, LC33, LC42, and LC43. Therefore, preliminary characterization was pursued for these lines. Interestingly, three of the candidates (LC27, LC30, and LC33) were all found to contain the same amiRNA sequence, indicating this is a robust target for further study (Table 1). This amiRNA (LC27/30/33; table 1) targets two leucine-rich repeat (LRR) family genes in *A. thaliana:* AT3G43740 and AT5G21090 (Berardini et al., 2015). In *A. thaliana,* LRR receptors are one of the most expansive families of cell surface receptors (Walker & Lease, 2010). LRRs are a leucine-rich structural motif, typically 22-29 amino acids long, that form a half-moon, concave structure that facilitates protein–protein interactions (Kobe & Deisenhofer, 1993; Kobe & Deisenhofer, 1995; Kobe & Kajava, 2001; Hothorn et al., 2011). These leucine-rich repeats form a series of beta-strands that are arranged in parallel, forming the curved half-moon shape. Based on 3D modeling of the protein structure, the LRR candidate (AT3G43740) has the typical LRR half-moon structure, but also seems to be part of a larger complex (Kelley et al., 2015). These LRR domains are found in a wide variety of characterized proteins, such as GHR1, BRI1, and FLS2 (Li & Chory, 1997; Hua et al., 2012; Hothorn et al., 2011). GHR1, a known player in guard cell CO_2 signaling, is a pseudo kinase (RLK-LRR); these receptor-like kinases (RLKs) make up a significant sub-class of LRR proteins (Sierla et al., 2018; Hõrak et al., 2016; Hua et al., 2012). There are multiple LRR proteins that are involved in stomatal development, such as the LRR

receptor-like protein (RLP), TOO MANY MOUTHS (TMM) (Rowe & Bergmann, 2010; Vráblová et al., 2017). LRR proteins are also known to be involved in disease resistance in plants, but the link between disease resistance signaling and either ABA or CO_2 has not been elucidated (McHale et al., 2006). Therefore, the LRR-targeting amiRNA candidate that has a CO_2-insensitive response phenotype could be implicated in guard cell CO_2 response signaling.

Since these genes have not yet been characterized in terms of the guard cell CO_2 signal transduction pathway for stomatal movements or stomatal development, our preliminary LRR-targeting amiRNA candidate characterization is a novel contribution to the field. Initial characterization of the LRR-targeting amiRNA candidate consists of gas exchange assays, stomatal index and density assays, and generation of a double-mutant CRISPR knockout (KO) plant. Gas exchange analysis compares the stomatal conductance of the candidate plant to wild-type. Stomatal index and density assays quantify the number of stomata per leaf for the candidate and wild-type, which shows whether stomatal conductance is impacted by the number of stomata. A double-mutant CRISPR plant has been designed to knockout the same two LRR family genes that the amiRNA plant targets, but will be more robust because it will fully eliminate the target genes. This double KO LRR mutant will be used to confirm the results garnered from the assays conducted with the amiRNA plants. Guide RNAs have been designed and cloning is ongoing for this candidate (Table 2).

The gas exchange results of the whole intact leaves of the LRR-targeting amiRNA plant suggest that the stomatal conductance response is partially impaired compared to wild-type (Figure 6). According to Stephan Ossowski and colleagues, since amiRNA constructs are randomly inserted into the *A. thaliana* genome, the observed gas exchange phenotype could be produced by the amiRNA insertion event disrupting gene function, rather than the amiRNA target gene

knockdown itself (Ossowski et al., 2018). Therefore, to overcome this limitation and ensure that the observed gas exchange phenotype is from an amiRNA-targeted degradation of the LRR transcripts (AT3G43740 and AT5G21090), rather than the insertion event, a new amiRNA line was designed. The amiRNA sequence was generated using Weigel Detlef's amiRNA designer tool to target the same LRR family genes (Ossowski et al., 2018). This new amiRNA is currently being cloned and transformed into Col-0 *A. thaliana* to give rise to a different random insertion event, but maintain the same knockdown gene-targets. This retransformation is essential to characterizing this candidate because if the partially impaired gas exchange phenotype, seen in Figure 5, is observed again with our new LRR-targeting transformant, it would suggest that the gene knockdown is indeed responsible for the phenotype, not the amiRNA insertion event. T-DNA lines have also been ordered for these LRR loci as a secondary approach to knock down gene function and eliminate any off-target effects from the amiRNA. The T-DNA lines will be crossed to obtain a double KO LRR mutant. The single and double LRR KO T-DNA lines can then be used to investigate if just one or both of the LRR genes are responsible for the observed phenotypes.

Stomatal development is impacted by atmospheric CO_2 concentration, with plants grown in elevated CO_2 conditions developing fewer stomata (Xu et al., 2016). To investigate whether the observed gas exchange phenotype is due to stomatal movements or development, a stomatal index and density assay was conducted on the LRR-targeting amiRNA candidate plant to measure the number of stomata per leaf area. The double-blind stomatal index and density assays show that there is a significant difference between the number of stomata in candidate LC27 and LC30 compared to WT (HsMYO) (Figure 17 and Figure 22) which suggests that the impaired gas exchange phenotype of the LRR-targeting amiRNA candidate plant is due to the larger size or lower number of stomata impairing the stomatal conductance, rather than the mechanical

movement of the stomatal opening and closure that is impacted. This suggests that the LRR candidate contains an amiRNA that is likely targeting genes involved in CO_2-mediated stomatal development, not stomatal movements. This requires further investigation. An impacted stomatal development phenotype suggests that the knockdown LRR family genes could be implicated in CO_2-mediated stomatal development. The DIC microscopy images show that the candidate LC30 had markedly larger stomata and pavement cells compared to WT (Figure 23). A more thorough stomatal size assay is ongoing.

Investigation into the protein–protein interactions of the LRR candidate genes, AT3G43740 and AT5G21090, was performed using published datasets and the ePlant web-based interface (Figure 24). An interactome was generated for AT3G43740 using ePlant. No interactors were found for locus AT5G21090. Research is ongoing using published datasets to generate an interactome that pulls from more databases to create an even more thorough picture of how these loci may be linked. The putative interactors found for LRR locus AT3G43740 were identified using TAIR: AT4G02010 as a protein kinase superfamily protein, AT4G27800 as TAP38/PPH1, and AT5G63770 as DGK2. PPH1 belongs to the PP2C-type phosphatase family and has been implicated in light acclimation (Shapiguzov et al., 2010). DGK2 is a member of the diaglycerol kinase gene family and encodes a functional diaglycerol kinase that is suggested to be involved in root elongation and leaf development (Angkawijaya et al., 2020). DGK2's involvement in leaf development is promising because this could link the candidate locus with development. Interestingly, OST1 was identified as a putative interactor of DGK2 (BioGRID; MIND). OST1 is an upstream regulator of SLAC1, the anion channel that responds to bicarbonate, the converted form of CO_2. OST1 has also been implicated in ABA signaling. This is a very promising interaction that putatively links the LRR candidate of interest to guard cell CO_2 signaling through OST1. It is

necessary to perform further bioinformatics analyses of proteomes, transcriptomes, and interactomes to see if this candidate is linked to any characterized players in stomatal development signaling, such as FAMA, MUTE, and ICE1/SCRM2, or any known factors involved in guard cell CO_2 signaling, including OST1, GHR1, and SLAC1.

Overall, this high-throughput complementary forward genetic screen identified a large number of promising candidates for elucidating novel factors involved in guard cell CO_2 signaling in *A. thaliana*. Currently, a double-mutant knockout CRISPR line, targeting the two LRR candidate genes: AT3G43740 and AT5G21090, is being generated to see if a complete knockout, as opposed to knockdown, will provide a more robust gas exchange phenotype and negate any off-target effects of the amiRNA construct. Additional time-resolved gas exchange as well as stomatal index and density experiments must be performed to confirm the observed phenotypes. Preliminary data suggests that this LRR candidate could be implicated in CO_2-mediated stomatal development which requires further investigation by analyzing stomatal density after growth in varying atmospheric CO_2 conditions. Another essential experiment for characterizing this LRR protein will be to investigate the other factors this protein may be interacting with. While putative interactors have been identified through published dataset analysis, these interactions must be validated *in planta*. These interactors will hopefully provide insight into how the LRR protein could be linked with the known components from the guard cell CO_2 signal transduction pathway in plants.

Further characterization of all candidates will likely provide better insights into CO_2-dependent signal transduction in guard cells. By gaining a better understanding of the CO_2 dependent response and signaling pathways in plants we can work towards developing transgenic plant lines that can better respond to elevated CO_2.

3.3 Conclusions:

In the present study, two redundancy-circumventing screens were pursued to identify new mutants and the underlying genes that regulate stomatal responses to low CO_2. The complementary forward genetic screen, performed in *Arabidopsis thaliana*, was conducted using two tools: the gain-of-function FOX-hunting plant line approach and a homologous gene silencing artificial miRNA (amiRNA) plant line approach. Both FOX-hunting and amiRNA plant lines were screened in conditions that specifically favored the identification of mutants involved in CO_2-mediated stomatal movements or stomatal development. A total of 43 amiRNA and 19 FOX-hunting candidates were identified and sequenced. One robust candidate, repeatedly identified in the screen, was an amiRNA line targeting two leucine-rich repeat (LRR) family genes: AT3G43740 and AT5G21090. This LRR candidate had a partially impaired gas exchange response compared to wild-type and had a lower stomatal count than wild-type, suggesting the observed phenotype is a product of a stomatal development mutation. The stomatal size of the LRR candidate was much larger than wild-type as well. The LRR locus, AT3G43740, was found to be putatively linked with a known guard cell CO_2 signaling player, OST1, through a protein–protein interactome investigation. Further research must be done to fully characterize this promising LRR candidate and validate the phenotypes observed in this study. Using this preliminary characterization as precedent, the remaining candidates identified from the forward genetic screens will be characterized in the future in order broaden our understanding of CO_2-mediated guard cell signaling.

4. METHODS:

4.1 Growth Conditions

The model organism used throughout this project was *Arabidopsis thaliana,* a dicot of the Columbia-0 (COL-0) ecotype (Hauser et al., 2019). The soil used was autoclaved Professional Growing Mix with added water to moisten soil for potting. For systemic insect control, one tablespoon of Marathon 1% granular (OHP, Inc. Bluffton, SC 29910 USA) was added per tray of soil after autoclaving. An additional tablespoon of Marathon was added to the tray at first water. The first water consisted of a 1.5 L water and 50x fertilizer solution poured onto the tray for bottom watering. The high-throughput screen used 3.5" pots filled to the edge with the above soil mix. T2 seeds were sown via suspension in 0.05% Agarose A media for homogenous syringe sowing. Seeds were stratified in a cold chamber for 3 days prior to sowing. The seedlings were covered using a high-dome plant cover to maintain higher humidity until they had fully established their first true leaves. T2 plants were grown in growth chambers at ambient CO_2 (400 ppm), 70% relative humidity (RH), 120-150 µmol/m2 light levels, and a 16h/8h photoperiod (Figure 25).

The re-screen was performed using BASTA selection for amiRNA seeds and Hygromycin selection for FOX seeds. First, the seeds were surface sterilized using a solution of 0.1% SDS for 10 minutes, 70% ethanol treatment for 2 minutes followed by 3 times wash with 100% ethanol, then fully dried before sowing. Seed stratification and selection was done by sowing sterilized seeds onto plates with media containing 5% Agarose, BASTA (25 µg/ml phosphinotricin, glufosinate ammonium), and ½ MS (Murashige and Skoog Basal w/Gamborg Vitamins) for amiRNA seeds, and 5% Agarose, 20 mg/L Hygromycin, and ½ MS plates for FOX seeds. The seeds were sown onto plates alongside controls, HsMYO and *ht1-2*. Then, the plates were micropore taped and incubated in a 4°C chamber for 3 days to stratify the seeds, which breaks any

seed dormancy and homogeneously initiates germination. The plates were moved to the ambient temperature growth chamber, following incubation, to continue germinating. Once seedlings had grown cotyledons and nubs of their first true leaves, the healthy BASTA-resistant T3 seedlings were transferred to pots using the same soil mix and pots described above. Re-screened T3 plants were grown in growth chambers at ambient CO_2 (400 ppm), 70% relative humidity (RH), 120-150 µmol/m^2 light levels, and a 12h/12h photoperiod. The seedlings were covered using a high-dome plant cover to maintain higher humidity so the plants could acclimate gradually down to ambient humidity (70% RH) without stress due to being grown on plates which maintain a very high RH.

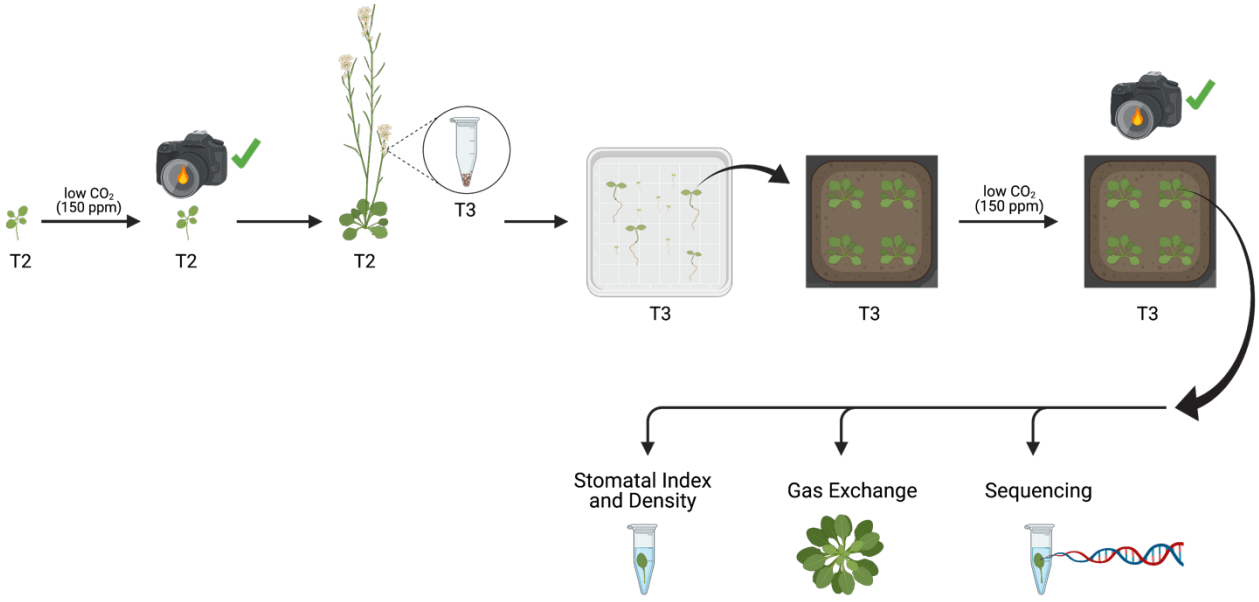

Figure 25: Screening protocol diagram. Created by the Author using BioRender.

4.2 Thermal imaging

The thermal imaging protocol was designed using Merlot et al., 2002 and Hauser et al., 2019). Thermal images were captured using a FLIR T650sc series thermal imaging camera outfitted with a 25° lens (FLIR Systems, Inc. Wilsonville, OR 97070 USA). The camera used an uncooled VoX microbolometer detector that is responsive to short wave infrared (7.5-13.0 μm). The specified temperature resolution was 0.25°C at room temperature. For the primary screen, the 3- to 4-week-old T2 plants were imaged following a 2-hour low-CO_2 (150 ppm) treatment in Conviron chambers. For the re-screen, the 5-week-old T3 plants were imaged following a 2-hour low-CO_2 (150 ppm) treatment in Conviron chambers (Figure 25). The camera was mounted 50 cm above the plant subject for imaging. Images were generated using manufacturer calibration. Brightfield images were extracted using FLIR tools. Raw IR images were converted to FITS (Flexible Image Transport System format) using ExaminIR software by FLIR for further temperature analysis. Temperatures were analyzed using ImageJ. An average of each individual leaf's temperature was taken to estimate the whole plant temperature.

4.3 Genomic DNA extraction

Genomic DNA (gDNA) extraction was performed as described in Edwards et al., 1991. Isolation of gDNA from *A. thaliana* leaf tissue was used for PCR amplification. The extraction steps were all done at room temperature. First, a disk of tissue was punched out of the plant leaf using a 1.5 mL Eppendorf tube. This starting material was ground using a pestle for 15 seconds and 400 μL of extraction buffer was added. This tube was vortexed for 5 seconds. Then, the tube was spun in a microfuge at max speed for 5 minutes to pellet debris. 300 μL of the supernatant was transferred to a fresh 1.5 mL Eppendorf tube. 300 μL of isopropanol was added to this tube,

mixed, and left at room temperature for 2 minutes. Then, the tube was spun at full speed for 5 minutes in a microfuge to pellet the DNA. The supernatant was discarded and then 750 µL of 80% ethanol was added to the tube. The tube was then spun at full speed for 5 minutes in the microfuge. The supernatant was removed completely and the pellet was dried gently by incubating the tube in a 37°C chamber for 3-5 minutes. Finally, 50 µL TE buffer was added to the tube and gently shaken to dissolve the pellet.

4.4 PCR Amplification of the amiRNA

Polymerase chain reactions (PCR) were performed to amplify the amiRNA inserts from the isolated candidate plant gDNA. Reactions of 25 µL total volume were performed using these materials: 2.5 µL 10X DreamTaq Buffer, 0.5 µL 10 mM dNTP Mix, 1 µL 10 µM 1119FP (forward primer), 1 µL 10 µM 1129RP (reverse primer), 1 µL gDNA, 0.1 µL DreamTaq DNA Polymerase, and 18.9 µL nuclease-free water. Samples were gently vortexed. Reactions were then placed in a thermal cycler using this program:

STEP	TEMPERATURE	TIME
Initial Denaturation	95°C	2 minutes
35 Cycles	95°C 55°C 72°C	30 seconds 30 seconds 60 seconds
Final Extension	72°C	10 minutes
Hold	10°C	∞

Then, agarose gel electrophoreses were performed. The samples were run on a 1% Agarose Gel with ethidium bromide (5 µL EtBr/100mL 1% agarose) alongside 5 µL of 1 kb ladder (Thermo Fisher Scientific, Waltham, MA USA 02451) and then visualized via UV light. Samples containing an amplified amiRNA were purified from gel and sent to sequencing.

4.5 Identification of the amiRNA

The sequencing data was aligned using Benchling (https://benchling.com/) to the miR319a sequence:

```
ctttgattggactgaagggagctccctctctctttgtattccaattttcttgattaatctttcc
tgcacaaaaacatgcttgatccactaagtgacatatatgctgccttcgtatatatagttctggta
aaattaacattttgggtttatctttatttaaggcatcgccatgcaaacacacgctcggacgcata
ttacacatgttcatacacttaatactcgctgttttgaattgatgttttaggaatatatatgtaga
gagagcttccttgagtccattcacaggtcgtgatatgattcaattagcttccgactcattcatcc
aaataccgagtcgccaaaattcaaactagactcgttaaatgaatgaatgatgcggtagacaaatt
ggatcattgattctctttgattggactgaagggagctccctctctctttgtattccaattttct
tgattaatctttcctgcacaaaaaca
```

The misalignment of 21nt at the beginning corresponds to the miRNA* and the end corresponds to the miRNA. Then, using the WMD3 website (http://wmd3.weigelworld.org/) the 21nt amiRNA sequence was searched under "target search" using these criteria: Genome = TAIR10 and Mismatches = 5. This search yielded the name and locus of the amiRNA.

4.6 LiCOR Gas Exchange Analysis

The stomatal conductance (g_s) was measured in the whole intact leaves of 5-week-old *Arabidopsis* plants from T3 candidate and control lines. The gas exchange analyzer used was a LiCOR 6400XT. The leaves, attached to whole intact plants, were clamped in the analyzer, and exposed to a variable CO_2 program. Leaves were equilibrated for an hour at ambient [CO_2] (400 ppm) at the relative humidity 70% before recording. After equilibration, the recording began, using the following variable CO_2 program: ambient CO_2 (400 ppm) for 30 minutes, low CO_2 (100 ppm) for 45 minutes, and high CO_2 (900 ppm) for 60 minutes (Figure 26).

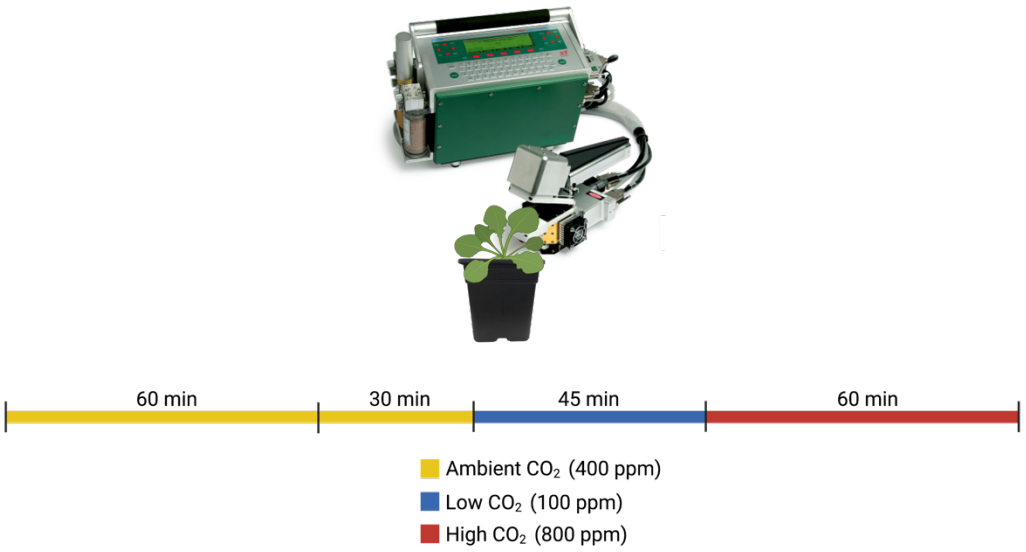

Figure 26: Gas exchange protocol. Created by the Author using BioRender.

4.7 Stomatal Index and Density Assay

Five plants per genotype were grown under 12h/12h light photoperiod and the 5th true leaf was harvested at 4-weeks-old. The leaf was clarified in clarity solution (1 acetic acid : 7 EtOH) to remove pigment for 24 hours, then softened in 1M KOH for 10 minutes, then suspended in DI water. The soft, clear leaf was then cut with a fresh razor blade along the primary vein of the leaf. The leaf without the vein was carefully lain on a fresh microscope slide with one drop of DI water and a cover slip was placed over the tissue. The abaxial side of the leaf was imaged via DIC microscopy using a Nikon Eclipse TS100 microscope camera and the Sharpcap 3.1 program. The leaf images were taken randomly around the abaxial side of the leaf at 40X magnification and 1200x1200 resolution (Figure 27). The TIFF file images were imported to ImageJ and counted with the Cell Counter ImageJ software. Prism was used to plot the data in box-whisker graphs and run a paired two-tailed t-test with Welch's correction for all candidates with WT (amiRNA-HsMYO). The assays were double-blinded by having one member blind the genotypes, another

harvest the tissue, another perform microscopy imaging, and another count the cells. The data was unblinded for statistical analysis and data processing.

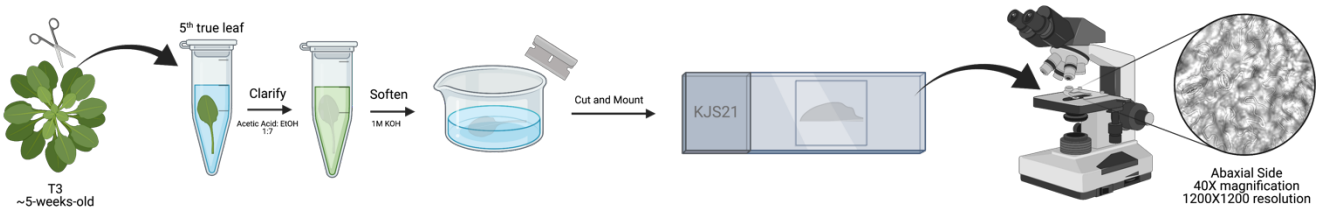

Figure 27: Stomatal index and density assay protocol. Created by the Author using BioRender.

4.7 Generating an interactome using published datasets

The ePlant Interaction Viewer was used to generate an interactome for the loci targeted by the amiRNA of interest (LC27/30/33), LRR family proteins: AT5G21090 & AT3G43740. The BAR Arabidopsis Interactions Viewer database provides the data for the interactome (Geisler-Lee et al., 2007), pulling from confirmed *Arabidopsis* interacting proteins found in the Biomolecular Interaction Network Database (BIND) (Popescu et al., 2007; Popescu et al., 2009), Arabidopsis Interactome (Arabidopsis Interactome Mapping Consortium, 2011), Membrane protein INteractome Database (MIND) (Frommer et al., 2009), and BioGRID (Stark et al., 2006). The viewer was built with CytoscapeJS using Javascript (Waese et al., 2017). All amiRNA loci targets are input to ePlant's web-based tools for visualizing functional genomics data for further characterization.

5. REFERENCES:

Amack, S. & Antunes, M. (2020). CaMV35S promoter – A plant biology and biotechnology workhorse in the era of synthetic biology. *Current Plant Biology.* https://doi.org/10.1016/j.cpb.2020.100179

Angkawijaya A. E., Nguyen V. C., Gunawan F., & Nakamura Y. (2020). A Pair of Arabidopsis Diacylglycerol Kinases Essential for Gametogenesis and Endoplasmic Reticulum Phospholipid Metabolism in Leaves and Flowers. *Plant Cell*, 32(8):2602-2620. doi: 10.1105/tpc.20.00251.

Arabidopsis Genome Initiative (2000). Analysis of the genome sequence of the flowering plant Arabidopsis thaliana. *Nature,* 408(1): 796–815.

Arabidopsis Interactome Mapping Consortium (2011). Evidence for network evolution in an Arabidopsis interactome map. Science (New York, N.Y.), 333(6042), 601–607. https://doi.org/10.1126/science.1203877

Azoulay-Shemer, T., Palomares, A., Bagheri, A., Israelsson-Nordstrom, M., Engineer, C. B., Bargmann, B. O., Stephan, A. B., & Schroeder, J. I. (2015). Guard cell photosynthesis is critical for stomatal turgor production, yet does not directly mediate CO2 - and ABA-induced stomatal closing. *The Plant journal : for cell and molecular biology,* 83(4), 567–581. https://doi.org/10.1111/tpj.12916

Bergmann, D. C. (2004). Integrating signals in stomatal development. *Current Opinion in Plant Biology,* 7(1):26–32. https://doi.org/10.1016/j.pbi.2003.10.001

Berardini T., Reiser L., Li D., Mezheritsky Y., Muller R., Strait E., & Huala E. (2015). The Arabidopsis Information Resource: Making and mining the "gold standard" annotated reference plant genome. *Wiley Periodicals, Inc.*, 53(1): 474–485. doi: 10.1002/dvg.22877

Bertolino, L. T., Caine, R. S., & Gray, J. E. (2019). Impact of Stomatal Density and Morphology on Water-Use Efficiency in a Changing World. *Frontiers in plant science,* 10, 225. https://doi.org/10.3389/fpls.2019.00225

Buckley, C. R., Caine, R. S., & Gray, J. E. (2020). Pores for Thought: Can Genetic Manipulation of Stomatal Density Protect Future Rice Yields?. *Frontiers in plant science,* 10, 1783. https://doi.org/10.3389/fpls.2019.01783

Carbonell, A., Takeda, A., Fahlgren, N., Johnson, S. C., Cuperus, J. T., & Carrington, J. C. (2014). New generation of artificial MicroRNA and synthetic trans-acting small interfering RNA vectors for efficient gene silencing in Arabidopsis. *Plant Physiology,* 165(1): 15-29. https://doi.org/10.1104/pp.113.234989

Ceciliato, P. H. O., Zhang, J., Liu, Q., Shen, X., Hu, H., Liu, C., Schäffner, A. R., & Schroeder, J. I. (2019). Intact leaf gas exchange provides a robust method for measuring the kinetics of stomatal conductance responses to abscisic acid and other small molecules in Arabidopsis and grasses. *Plant Methods,* 38(1): 15. https://doi.org/10.1186/s13007-019-0423-y

Chater, C. C. C., Caine, R. S., Fleming, A. J., & Gray, J. E. (2017). Origins and evolution of stomatal development. *Plant Physiology,* 174(2): 624–638. https://doi.org/10.1104/pp.17.00183

Cutler S, & McCourt P. (2005) Dude, where's my phenotype? Dealing with redundancy in signaling networks. *Plant Physiology.* 138(2):558-9. doi: 10.1104/pp.104.900152.

Demir, F., Horntrich, C., Blachutzik, J. O., Scherzer, S., Reinders, Y., Kierszniowska, S., Schulze, W. X., Harms, G. S., Hedrich, R., Geiger, D., & Kreuzer, I. (2013). Arabidopsis nanodomain-delimited ABA signaling pathway regulates the anion channel SLAH3. *Proceedings of the National Academy of Sciences of the United States of America*, 110(20), 8296–8301. https://doi.org/10.1073/pnas.1211667110

Dong, H., Bai, L., Zhang, Y., Zhang, G., Mao, Y., Min, L., Xiang, F., Qian, D., Zhu, X., & Song, C. P. (2018). Modulation of Guard Cell Turgor and Drought Tolerance by a Peroxisomal Acetate-Malate Shunt. *Molecular plant,* 11(10), 1278–1291. https://doi.org/10.1016/j.molp.2018.07.008

Engineer, C. B., Ghassemian, M., Anderson, J. C., Peck, S. C., Hu, H., & Schroeder, J. I. (2014). Carbonic anhydrases, EPF2 and a novel protease mediate CO2 control of stomatal development. *Nature*, 513(7517): 246–250. https://doi.org/10.1038/nature13452

Edwards, K., Johnstone, C., & Thompson, C. (1991). A simple and rapid method for the preparation of plant genomic DNA for PCR analysis. *Nucleic acids research,* 19(6), 1349. https://doi.org/10.1093/nar/19.6.1349

Engineer, C. B., Hashimoto-Sugimoto, M., Negi, J., Israelsson-Nordström, M., Azoulay-Shemer, T., Rappel, W. J., Iba, K., & Schroeder, J. I. (2016). CO2 Sensing and CO2 Regulation of Stomatal Conductance: Advances and Open Questions. *Plant Science,* 21(1): 16–30. https://doi.org/10.1016/j.tplants.2015.08.014

Wang, F. F., Lian, H. L., Kang, C. Y., & Yang, H. Q. (2010). Phytochrome B is involved in mediating red light-induced stomatal opening in Arabidopsis thaliana. *Molecular plant,* 3(1), 246–259. https://doi.org/10.1093/mp/ssp097

Frommer, W. B., Davidson, M. W., & Campbell, R. E. (2009). Genetically encoded biosensors based on engineered fluorescent proteins. *Chemical Society reviews*, 38(10), 2833–2841. https://doi.org/10.1039/b907749a

Geisler-Lee, J., O'Toole, N., Ammar, R., Provart, N. J., Millar, A. H., & Geisler, M. (2007). A predicted interactome for Arabidopsis. *Plant physiology,* 145(2), 317–329. https://doi.org/10.1104/pp.107.103465

Harrison, E. L., Arce Cubas, L., Gray, J. E., & Hepworth, C. (2020). The influence of stomatal morphology and distribution on photosynthetic gas exchange. *Plant Journal*, 101(4): 768-779. https://doi.org/10.1111/tpj.14560

Hauser, F., Ceciliato, P., Lin, Y. C., Guo, D., Gregerson, J. D., Abbasi, N., & Schroeder, J. I. (2019). A seed resource for screening functionally redundant genes and isolation of new mutants impaired in CO2 and ABA responses. *Journal of experimental botany*, 70(2): 641–651. doi:10.1093/jxb/ery363

Hauser, F., Chen, W., Deinlein, U., Chang, K., Ossowski, S., Fitz, J., & Schroeder, J. I. (2013). A genomic-scale artificial microRNA library as a tool to investigate the functionally redundant gene space in Arabidopsis. *The Plant cell*, 25(8): 2848–2863. doi:10.1105/tpc.113.112805

Hauser, F., Li, Z., Waadt, R., & Schroeder, J. I. (2017). SnapShot: Abscisic Acid Signaling. *Cell*, 171(7): 1708. https://doi.org/10.1016/j.cell.2017.11.045

Hashimoto, M., Negi, J., Young, J., Israelsson, M., Schroeder, J. I., & Iba, K. (2006). Arabidopsis HT1 kinase controls stomatal movements in response to CO2. *Nature Cell Biology,* 8(4): 391–397. https://doi.org/10.1038/ncb1387

Hetherington, A. M., & Woodward, F. I. (2003). The role of stomata in sensing and driving environmental change. *Nature*, 424(6951): 901-908. https://doi.org/10.1038/nature01843

Hiyama, A., Takemiya, A., Munemasa, S., Okuma, E., Sugiyama, N., Tada, Y., Murata, Y., & Shimazaki, K. I. (2017). Blue light and CO2 signals converge to regulate light-induced stomatal opening. *Nature Communications,* 8(1): 1284. https://doi.org/10.1038/s41467-017-01237-5

Hõrak, H., Sierla, M., Tõldsepp, K., Wang, C., Wang, Y. S., Nuhkat, M., Valk, E., Pechter, P., Merilo, E., Salojärvi, J., Overmyer, K., Loog, M., Brosché, M., Schroeder, J. I., Kangasjärvi, J., & Kollist, H. (2016). A dominant mutation in the ht1 kinase uncovers roles of MAP kinases and GHR1 in CO2-induced stomatal closure. *Plant Cell*, 28(10), 2493–2509. https://doi.org/10.1105/tpc.16.00131

Hothorn, M., Belkhadir, Y., Dreux, M., Dabi, T., Noel, J. P., Wilson, I. A., & Chory, J. (2011). Structural basis of steroid hormone perception by the receptor kinase BRI1. *Nature*, 474(7352), 467–471. https://doi.org/10.1038/nature10153

Hsu, P. K., Takahashi, Y., Munemasa, S., Merilo, E., Laanemets, K., Waadt, R., Pater, D., Kollist, H., & Schroeder, J. I. (2018). Abscisic acid-independent stomatal CO2 signal transduction pathway and convergence of CO2 and ABA signaling downstream of OST1

kinase. *Proceedings of the National Academy of Sciences of the United States of America,* 115(42), E9971–E9980. https://doi.org/10.1073/pnas.1809204115

Hu, H., Boisson-dernier, A., Israelsson-nordström, M., Xue, S., Ries, A., Godoski, J., Kuhn, J. M., & Julian, I. (2010). Carbonic anhydrases are upstream regulators of CO2-controlled stomatal movements in guard cells. *Nature Cell Biology,* 2(1): 87-93. https://doi.org/10.1038/ncb2009.Carbonic

Hua, D., Wang, C., He, J., Liao, H., Duan, Y., Zhu, Z., Guo, Y., Chen, Z., & Gong, Z. (2012). A plasma membrane receptor kinase, GHR1, mediates abscisic acid- and hydrogen peroxide-regulated stomatal movement in Arabidopsis. *The Plant cell,* 24(6), 2546–2561. https://doi.org/10.1105/tpc.112.100107

Ichikawa, T., Nakazawa, M., Kawashima, M., Iizumi, H., Kuroda, H., Kondou, Y., Tsuhara, Y., Suzuki, K., Ishikawa, A., Seki, M., Fujita, M., Motohashi, R., Nagata, N., Takagi, T., Shinozaki, K., & Matsui, M. (2006). The FOX hunting system: An alternative gain-of-function gene hunting technique. *Plant Journal,* 48(6): 974-85. https://doi.org/10.1111/j.1365-313X.2006.02924.x

Jakobson, L., Vaahtera, L., Tõldsepp, K., Nuhkat, M., Wang, C., Wang, Y. S., Hõrak, H., Valk, E., Pechter, P., Sindarovska, Y., Tang, J., Xiao, C., Xu, Y., Gerst Talas, U., García-Sosa, A. T., Kangasjärvi, S., Maran, U., Remm, M., Roelfsema, M. R. G., Hu, H., Kangasjärvi, J., Loog, M., Schroeder, J. I., Kollist, H., & Brosché, M. (2016). Natural Variation in Arabidopsis Cvi-0 Accession Reveals an Important Role of MPK12 in Guard Cell CO2 Signaling. *PLoS Biology,* 14(12), 2000322. https://doi.org/10.1371/journal.pbio.2000322

Keeling, C. D., Bacastow, R. B., & Bainbridge, A. E. (1976). Atmospheric carbon dioxide variations at Mauna Loa Observatory, Hawaii. *TELLUS,* 28(6): 538-51. https://doi.org/10.3402/tellusa.v28i6.11322

Kelley, L. A., Mezulis, S., Yates, C. M., Wass, M. N., & Sternberg, M. J. (2015). The Phyre2 web portal for protein modeling, prediction and analysis. *Nature protocols,* 10(6), 845–858. https://doi.org/10.1038/nprot.2015.053

Kim, T.-H., Böhmer, M., Hu, H., Nishimura, N., & Schroeder, J. I. (2010). Guard Cell Signal Transduction Network: Advances in Understanding Abscisic Acid, CO 2 , and Ca 2+ Signaling. *Annual Review of Plant Biology,* 61(1): 561-91. https://doi.org/10.1146/annurev-arplant-042809-112226

Kobe, B., & Deisenhofer, J. (1995). A structural basis of the interactions between leucine-rich repeats and protein ligands. *Nature*, 374(6518), 183–186. https://doi.org/10.1038/374183a0

Kobe, B., & Deisenhofer, J. (1993). Crystal structure of porcine ribonuclease inhibitor, a protein with leucine-rich repeats. *Nature*, 366(6457), 751–756. https://doi.org/10.1038/366751a0

Kobe, B., & Kajava, A. V. (2001). The leucine-rich repeat as a protein recognition motif. *Current opinion in structural biology,* 11(6), 725–732. https://doi.org/10.1016/s0959-440x(01)00266-4

Kollist, H., Nuhkat, M., & Roelfsema, M. R. G. (2014). Closing gaps: Linking elements that control stomatal movement. *New Phytologist,* 203(1): 44-62. https://doi.org/10.1111/nph.12832

Koornneef, M., & Meinke, D. (2010). The development of Arabidopsis as a model plant. *Plant Journal,* 61(6): 909-21. https://doi.org/10.1111/j.1365-313X.2009.04086.x

Lawson, T., & Blatt, M. R. (2014). Stomatal size, speed, and responsiveness impact on photosynthesis and water use efficiency. *Plant Physiology,* 164(4): 1556-70. https://doi.org/10.1104/pp.114.237107

Li, J., & Chory, J. (1997). A putative leucine-rich repeat receptor kinase involved in brassinosteroid signal transduction. *Cell,* 90(5), 929–938. https://doi.org/10.1016/s0092-8674(00)80357-8

Ma, Y., Szostkiewicz, I., Korte, A., Moes, D., Yang, Y., Christmann, A., & Grill, E. (2009). Regulators of PP2C phosphatase activity function as abscisic acid sensors. *Science*, 324(5930): 1064-8. https://doi.org/10.1126/science.1172408

Matrosova A., Bogireddi H., Mateo-Peñas A., Hashimoto-Sugimoto M., Iba K., Schroeder J. I., & Israelsson-Nordström M. (2015). The HT1 protein kinase is essential for red light-induced stomatal opening and genetically interacts with OST1 in red light and CO2 -induced stomatal movement responses. *New Phytologist* 208, 1126–1137.

McHale, L., Tan, X., Koehl, P., & Michelmore R. (2006). Plant NBS-LRR proteins: adaptable guards. *Genome Biology,* 7(1):212. https://doi.org/10.1186/gb-2006-7-4-212

Merlot, S., Mustilli, A., Genty, B., North, H., Lefebvre, V., Sotta, B., Vavasseur, A., Giraudat, J. (2002). Use of infrared thermal imaging to isolate Arabidopsis mutants defective in stomatal regulation. *The Plant Journal,* 30(5), 601–609. https://doi.org/10.1046/j.1365-313X.2002.01322.x

Metcalfe, C. R. & Chalk, L. (1950). *Anatomy of the dicotyledons.* (Vol. 1 and II) Oxford Press.

Mora, C., Spirandelli, D., Franklin, E. C., Lynham, J., Kantar, M. B., Miles, W., Smith, C. Z., Freel, K., Moy, J., Louis, L. V., Barba, E. W., Bettinger, K., Frazier, A. G., Colburn IX, J. F., Hanasaki, N., Hawkins, E., Hirabayashi, Y., Knorr, W., & Little, C. M., Hunter, C. L. (2018). Broad threat to humanity from cumulative climate hazards intensified by greenhouse gas emissions. *Nature Climate Change,* 8(1): 1062–71. https://doi.org/10.1038/s41558-018-0315-6

Negi, J., Matsuda, O., Nagasawa, T., Oba, Y., Takahashi, H., Kawai-Yamada, M., Uchimiya, H., Hashimoto, M., & Iba, K. (2008). CO2 regulator SLAC1 and its homologues are essential for anion homeostasis in plant cells. Nature, 452(7186), 483–486. https://doi.org/10.1038/nature06720

Nowak, D. J., & Crane, D. E. (2002). Carbon storage and sequestration by urban trees in the USA. *Environmental Pollution*, 116(3): 381-9. https://doi.org/10.1016/S0269-7491(01)00214-7

Nunes, T., Zhang, D., & Raissig, M. T. (2020). Form, development and function of grass stomata. *The Plant journal : for cell and molecular biology,* 101(4), 780–799. https://doi.org/10.1111/tpj.14552

Ossowski S., Fitz J., Schwab R., Riester M., & Weigel D. (2018). Personal Communication.

Ossowski, S., Schwab, R., & Weigel, D. (2008). Gene silencing in plants using artificial microRNAs and other small RNAs. *Plant Journal,* 53(4): 674-90. https://doi.org/10.1111/j.1365-313X.2007.03328.x

Park, S. Y., Fung, P., Nishimura, N., Jensen, D. R., Fujii, H., Zhao, Y., Lumba, S., Santiago, J., Rodrigues, A., Chow, T. F. F., Alfred, S. E., Bonetta, D., Finkelstein, R., Provart, N. J., Desveaux, D., Rodriguez, P. L., McCourt, P., Zhu, J. K., Schroeder, J. I., & Cutler, S. R. (2009). Abscisic acid inhibits type 2C protein phosphatases via the PYR/PYL family of START proteins. *Science,* 324(5930): 1068-71. https://doi.org/10.1126/science.1173041

Peterson, K. M., Rychel, A. L., & Torii, K. U. (2010). Out of the mouths of plants: the molecular basis of the evolution and diversity of stomatal development. *The Plant cell*, 22(2), 296–306. https://doi.org/10.1105/tpc.109.072777

Popescu, S. C., Popescu, G. V., Bachan, S., Zhang, Z., Seay, M., Gerstein, M., Snyder, M., & Dinesh-Kumar, S. P. (2007). Differential binding of calmodulin-related proteins to their targets revealed through high-density Arabidopsis protein microarrays. *Proceedings of the National Academy of Sciences of the United States of America,* 104(11), 4730–4735. https://doi.org/10.1073/pnas.0611615104

Popescu, S. C., Popescu, G. V., Bachan, S., Zhang, Z., Gerstein, M., Snyder, M., & Dinesh-Kumar, S. P. (2009). MAPK target networks in Arabidopsis thaliana revealed using functional protein microarrays. *Genes & development,* 23(1), 80–92. https://doi.org/10.1101/gad.1740009

Rajeevkumar, S., Anunanthini, P., & Sathishkumar, R. (2015). Epigenetic silencing in transgenic plants. *Frontiers in plant science,* 6, 693. https://doi.org/10.3389/fpls.2015.00693

Rowe, M. H., & Bergmann, D. C. (2010). Complex signals for simple cells: the expanding ranks of signals and receptors guiding stomatal development. *Current Opinion in Plant Biology*, 13(5): 548-555. https://doi.org/10.1016/j.pbi.2010.06.002

Santelia, D., & Lawson, T. (2016). Rethinking guard cell metabolism. *Plant Physiology,* 172(3): 1371-92. https://doi.org/10.1104/pp.16.00767

Schroeder J.I., Allen G.J., Hugouvieux V., Kwak J.M., & Waner D. (2001). Guard cell signal transduction*. Annu. Rev. Plant Physiol. Plant Mol. Biol*., 52: 627–58.

Schulze, E. D., Lange, O. L., Kappen, L., Buschbom, U., & Evenari, M. (1973). Stomatal responses to changes in temperature at increasing water stress. *Planta*, 110(1):29–42. https://doi.org/10.1007/BF00386920

Schwab, R., Ossowski, S., Riester, M., Warthmann, N., & Weigel, D. (2006). Highly specific gene silencing by artificial microRNAs in Arabidopsis. *Plant Cell,* 18(5), 1121–1133. https://doi.org/10.1105/tpc.105.039834

Scripps Institution of Oceanography. (2018). *The Keeling Curve*. UC San Diego.

Shapiguzov, A., Ingelsson, B., Samol, I., Andres, C., Kessler, F., Rochaix, J. D., Vener, A. V., & Goldschmidt-Clermont, M. (2010). The PPH1 phosphatase is specifically involved in LHCII dephosphorylation and state transitions in Arabidopsis. *Proceedings of the National Academy of Sciences of the United States of America,* 107(10), 4782–4787. https://doi.org/10.1073/pnas.0913810107

Sierla, M., Hõrak, H., Overmyer, K., Waszczak, C., Yarmolinsky, D., Maierhofer, T., Vainonen, J. P., Salojärvi, J., Denessiouk, K., Laanemets, K., Tõldsepp, K., Vahisalu, T., Gauthier, A., Puukko, T., Paulin, L., Auvinen, P., Geiger, D., Hedrich, R., Kollist, H., & Kangasjärvi, J. (2018). The Receptor-like Pseudokinase GHR1 Is Required for Stomatal Closure. *The Plant cell,* 30(11), 2813–2837. https://doi.org/10.1105/tpc.18.00441

Stark, C., Breitkreutz, B. J., Reguly, T., Boucher, L., Breitkreutz, A., & Tyers, M. (2006). BioGRID: a general repository for interaction datasets. *Nucleic acids research,* 34(Database issue), D535–D539. https://doi.org/10.1093/nar/gkj109

Talbott, L. D., Shmayevich, I. J., Chung, Y., Hammad, J. W., & Zeiger, E. (2003). Blue light and phytochrome-mediated stomatal opening in the npq1 and phot1 phot2 mutants of Arabidopsis. *Plant physiology,* 133(4), 1522–1529. https://doi.org/10.1104/pp.103.029587

Tõldsepp, K., Zhang, J., Takahashi, Y., Sindarovska, Y., Hõrak, H., Ceciliato, P. H. O., Koolmeister, K., Wang, Y.-S., Vaahtera, L., Jakobson, L., Yeh, C.-Y., Park, J., Brosche, M., Kollist, H., & Schroeder, J. I. (2018). Mitogen-activated protein kinases MPK4 and MPK12 are key components mediating CO2-induced stomatal movements. *The Plant Journal*, 96(5), 1018–1035. https://doi.org/10.1111/tpj.14087

Viczián, A., Ádám, É., Staudt, A. M., Lambert, D., Klement, E., Romero Montepaone, S., Hiltbrunner, A., Casal, J., Schäfer, E., Nagy, F., & Klose, C. (2020). Differential

phosphorylation of the N-terminal extension regulates phytochrome B signaling. The *New phytologist,* 225(4), 1635–1650. https://doi.org/10.1111/nph.16243

Vráblová, M., Vrábl, D., Hronková, M., Kubásek, J., & Šantrůček, J. (2017). Stomatal function, density and pattern, and CO2 assimilation in Arabidopsis thaliana tmm1 and sdd1-1 mutants. *Plant Biology,* 19(5), 689–701. https://doi.org/10.1111/plb.12577

Waese, J., Fan, J., Pasha, A., Yu, H., Fucile, G., Shi, R., Cumming, M., Kelley, L. A., Sternberg, M. J., Krishnakumar, V., Ferlanti, E., Miller, J., Town, C., Stuerzlinger, W., & Provart, N. J. (2017). ePlant: Visualizing and Exploring Multiple Levels of Data for Hypothesis Generation in Plant Biology. *The Plant cell,* 29(8), 1806–1821. https://doi.org/10.1105/tpc.17.00073

Walker J. C. & Lease K. A. (2010). *Handbook of Cell Signaling: The Leucine-Rich Repeat Receptor Protein Kinases of Arabidopsis thaliana – a Paradigm for Plant LRR Receptors.* (2nd ed.) Academic Press.

Wang, C., Hu, H., Qin, X., Zeise, B., Xu, D., Rappel, W. J., Boron, W. F., & Schroeder, J. I. (2015). Reconstitution of CO2 regulation of SLAC1 anion channel and function of CO2-permeable PIP2;1 aquaporin as CARBONIC ANHYDRASE4 interactor. *Plant Cell,* 28(2), 568–582. https://doi.org/10.1105/tpc.15.00637

Wang, F. F., Lian, H. L., Kang, C. Y., & Yang, H. Q. (2010). Phytochrome B is involved in mediating red light-induced stomatal opening in Arabidopsis thaliana. *Molecular plant,* 3(1), 246–259. https://doi.org/10.1093/mp/ssp097

Weyers, J. D. B., Fitzsimons, P. J., Mansey, G. M., & Martin, E. S. (1983). Guard cell protoplasts – Aspects of work with an important new research tool. *Physiologia Plantarum,* 58(3): 331-9. https://doi.org/10.1111/j.1399-3054.1983.tb04189.x

Willmer, C., & Fricker, M. (1996). Stomatal responses to environmental factors. *Stomata*, 126–191. https://doi.org/10.1007/978-94-011-0579-8_6

Woodward FI. (1987). Stomatal numbers are sensitive to CO2 increases from preindustrial levels. *Nature,* 327:617–18.

Xu, Z., Jiang, Y., Jia, B., & Zhou, G. (2016). Elevated-CO2 Response of Stomata and Its Dependence on Environmental Factors. *Frontiers in plant science,* 7, 657. https://doi.org/10.3389/fpls.2016.00657

Xue, S., Hu, H., Ries, A., Merilo, E., Kollist, H., & Schroeder, J. I. (2011). Central functions of bicarbonate in S-type anion channel activation and OST1 protein kinase in CO2 signal transduction in guard cell. *EMBO Journal,* 30(8), 1645–1658. https://doi.org/10.1038/emboj.2011.68

Yang, J., Li, C., Kong, D., Guo, F., & Wei, H. (2020). Light-Mediated Signaling and Metabolic Changes Coordinate Stomatal Opening and Closure. *Frontiers in plant science,* 11, 601478. https://doi.org/10.3389/fpls.2020.601478

Yibing Wang, Geoffrey Holroyd, Alistair M Hetherinton, & Carl K-Y Ng. (2004). Seeing “cool” and ’hot’--infrared thermography as a tool for non-invasive, high-throughput screening of Arabidopsis guard cell signalling mutants. *Journal of Experimental Botany,* 1(22), 8–12. https://doi.org/10.1093/jxb

Zhang, J., De-oliveira-Ceciliato, P., Takahashi, Y., Schulze, S., Dubeaux, G., Hauser, F., Azoulay-Shemer, T., Tõldsepp, K., Kollist, H., Rappel, W. J., & Schroeder, J. I. (2018). Insights into the Molecular Mechanisms of CO2-Mediated Regulation of Stomatal Movements. *Current Biology*, 28(23): 1356-63. https://doi.org/10.1016/j.cub.2018.10.

Zheng, Y., Li, F., Hao, L., Yu, J., Guo, L., Zhou, H., Ma, C., Zhang, X., & Xu, M. (2019). Elevated CO2 concentration induces photosynthetic down-regulation with changes in leaf structure, non-structural carbohydrates and nitrogen content of soybean. *BMC Plant Biology,* 19(1): 255. https://doi.org/10.1186/s12870-019-1788-9